

ARTICLE TYPE

A shape optimization algorithm based on directional derivatives for three-dimensional contact problems

Bastien Chaudet-Dumas

¹Section of Mathematics, University of Geneva, Switzerland

Correspondence

*Bastien Chaudet-Dumas. Email: bastien.chaudet@unige.ch

Summary

This work deals with shape optimization for contact mechanics. More specifically, the linear elasticity model is considered under the small deformations hypothesis, and the elastic body is assumed to be in contact (sliding or with Tresca friction) with a rigid foundation. The mathematical formulations studied are two regularized versions of the original variational inequality: the penalty formulation and the augmented Lagrangian formulation. In order to get the shape derivatives associated to those two non-differentiable formulations, we follow an approach based on directional derivatives^{1,2}. This allows us to develop a gradient-based topology optimization algorithm, built on these derivatives and a level-set representation of shapes. The algorithm also benefits from a mesh-cutting technique, which gives an explicit representation of the shape at each iteration, and enables us to apply the boundary conditions strongly on the contact zone. The different steps of the method are detailed. Then, to validate the approach, some numerical results on two-dimensional and three-dimensional benchmarks are presented.

KEYWORDS:

shape optimization, level-set method, contact mechanics, Tresca friction, linear elasticity, penalty method, augmented Lagrangian method

1 | INTRODUCTION

Structural optimization has become an integral part of industrial conception, with applications in more and more challenging mechanical contexts. Those mechanical contexts often lead to complex mathematical formulations involving non-linearities and/or non-differentiabilities, which causes many difficulties when considering the associated shape optimization problem. This is the reason why this topic has been widely studied for the past fifty years in various research fields such as engineering, optimization and numerical analysis. In this article, we are interested in finding the optimal shape of a body in contact with a rigid foundation, in the sense that this shape must maximize or minimize some given mechanical criterion. The deformable body is assumed to be made of a linear elastic material and the contact model considered is either frictionless (sliding) or with Tresca friction.

The structural optimization problem takes the form of a constrained optimization problem in infinite dimension, one of the constraints being the state equation modeling the mechanical equilibrium (usually written as a variational formulation). In general, the numerical resolution of this optimization problem is tackled using gradient based optimization algorithms, which of course require the expressions of the shape derivatives. There exist two main families of approaches to address this issue.

Following the usual terminology^{3,4}, we first mention the paradigm *optimize-then-discretize*, which consists in writing the optimality conditions associated to the state equation in the infinite dimensional setting, then discretizing this state equation and the optimality conditions obtained⁵. The second paradigm, referred to as *discretize-then-optimize*, consists in discretizing the state equation first, then write the related shape optimization problem in finite dimension and derive the associated optimality conditions⁶. Here, we follow the first one, and we compute our shape derivatives using Hadamard's boundary variation method. Note that, since the pioneer work of Hadamard⁷, there have been many studies following this approach^{8,9,10,11,12,13}.

Another key issue in shape optimization is the representation of the shapes. In this article, we use a representation based on the level-set method, as it was first exposed in the 2000's^{14,15,16,5} in the context of structural optimization, and also in the context of topology optimization^{17,18} using the notion topological derivative. The use of a level-set function ϕ is very interesting in practice as it enables us to deal with geometric deformations of the domain by simply solving an advection equation, and it also allows topology changes. However, when using this technique, as in the case of density methods⁶, we do not have a sharp representation of the interface $\partial\Omega = \{\phi = 0\}$ ¹⁹. Originally, the authors got around this difficulty by enforcing the boundary conditions approximately on $\partial\Omega$, by means of a regularized Heaviside function. In the same spirit, we also mention shape optimization algorithms that use immersed boundary techniques which are very efficient to handle boundary conditions when no mesh of the boundary is available. Among these algorithms, some use the very popular XFEM method^{20,21}. Here, we choose a different approach which consists in coupling the level-set method with a conformal discretization. This means that we work with a description of the shape which is not only implicit (by means of ϕ) but also explicit (by means of an actual mesh for the discrete shape). There have been various works in this direction^{22,23,24,25}, some of which even use a boundary element method to solve the mechanical problem²⁶. Obviously, this approach is more expensive as it involves some remeshing procedure at each shape optimization iteration. However, it enables us to limitate the numerical resolution of the mechanical problem to Ω only, and to apply exactly the boundary conditions on $\partial\Omega$, which is crucial in the case of contact mechanics as the quality of the obtained solution highly depends on the accuracy in the neighbourhood of the contact zone. In order to build this explicit representation of Ω , we propose a new mesh cutting technique based on a quadratic interpolation of the level-set function, which is very simple, not very costly, and gives a rather smooth representation of the shapes.

Given the assumptions made on the material and on the friction model, the mathematical formulation associated to our contact problem takes the form of a variational inequality of the second kind, for which existence, uniqueness and regularity of the solution have been established^{27,28}. In the context of shape optimization, this formulation is not really convenient as it is not differentiable with respect to the shape because of the projection operators involved in the expression of the contact boundary conditions. This issue may be addressed in different ways. First, it is possible to introduce a weaker notion of differentiability, called conical differentiability²⁹, and work with this notion to derive the associated first order optimality conditions. This approach has been applied to our problem in two dimensions³⁰, but the expressions of the shape derivatives are not very usable in numerical practice. Second, following the *discretize-then-optimize* paradigm, it is possible to discretize the formulation, then use the tools from subdifferential calculus. This approach has been successfully applied in the context of shape optimization for elastic bodies in frictional contact with a plane^{31,32,33,34}. Finally, a popular approach among the mechanical engineering community is to consider a regularized but approximate formulation of the original variational inequality such as the penalty formulation or the augmented Lagrangian formulation. This new formulation usually takes the form of a non-linear non-differentiable variational formulation. Regularizing all non-smooth functions leads to an approximate formulation that is classically shape differentiable. There have been a few works in this direction using the penalty method³⁵, even recently³⁶. In this last reference, the authors use the level-set method and they compute shape derivatives for the continuous problem in two and three dimensions, but do not take into account a possible gap between the bodies in contact. As for the augmented Lagrangian method, there exists a mathematical analysis of shape sensitivity together with the associated numerical results for some specific cost functionals in two dimensions^{37,38}, but these studies are limited to parametric shape optimization (using B-splines) in the frictionless case. Finally, let us also mention a very recent work³⁹ where the authors consider the geometric shape optimization of a rolling structure in frictional contact with a plane in two and three dimensions, without optimizing the contact zone. The contact is modeled using Nitsche's method⁴⁰, and they use a level-set representation of the shapes, with a fictitious domain approach close to XFEM to solve the mechanical formulation.

In the present work, we propose a shape optimization method that optimizes the whole boundary of the domain (including the contact zone) as well as its topology in the three-dimensional frictional case. Moreover, we consider the general case of a structure in contact with a non necessarily plane rigid object, and we take into account a possible gap between the two bodies. The contact formulations studied are the penalty formulation and the augmented Lagrangian formulation, without any additional regularization procedure. Our approach relies on an original and rigorous computation of the shapes derivatives based on the

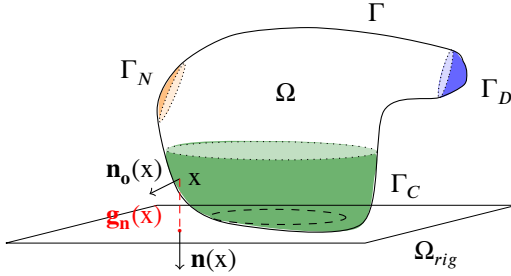


FIGURE 1 Elastic body in contact with a rigid foundation.

directional derivatives of the non-smooth functions that appear in these formulations^{1,2}. Furthermore, thanks to our novel mesh-cutting technique, the numerical method presented benefits from an explicit representation of the shape without spending too much computational time on the remeshing procedure. This enables us to enforce the contact condition exactly on the boundary.

This article is structured as follows. Section 2 presents the mechanical problem and its different formulations: the original formulation and the two regularized formulations studied (penalty and augmented Lagrangian). In section 3 we discuss the shape optimization problem, in particular we derive the shape derivatives associated to each of the two regularized formulations. Section 4 gives a detailed description of the numerical shape optimization algorithm, in which the mesh-cutting technique is presented and discussed. Finally, some numerical results are presented in section 5. These results help validate the approach and allow for comparison between the penalty method and the augmented Lagrangian method.

2 | MECHANICAL PROBLEM FORMULATION

We are considering in \mathbb{R}^d , $d \in \{2, 3\}$, the problem of a deformable body coming in contact with a rigid foundation under the action of body forces and surface loads. We denote by Ω the domain representing the deformable body and by Ω_{rig} the rigid foundation. Let Γ_D be the part of the boundary where a homogeneous Dirichlet condition applies (blue part), Γ_N the part where a non-homogeneous Neumann condition τ applies (orange part), Γ_C the potential contact zone (green part), and Γ the rest of the boundary, which is free of any constraint (i.e. homogeneous Neumann boundary condition). Those four parts are mutually disjoint and we have: $\overline{\Gamma_D} \cup \overline{\Gamma_N} \cup \overline{\Gamma_C} \cup \overline{\Gamma} = \partial\Omega$, as depicted in Figure 1.

Remark 1. In this paper, vector and tensor valued functions will be represented in bold font to distinguish them from scalar valued functions.

The outward normal to Ω is denoted by \mathbf{n}_0 . Similarly, the inward normal to Ω_{rig} is denoted by \mathbf{n} . We also introduce the space $\mathbf{X} := \mathbf{H}_{\Gamma_D}^1(\Omega) = \{\mathbf{v} \in (H^1(\Omega))^d \mid \mathbf{v}|_{\Gamma_D} = 0\}$, and \mathbf{X}^* its dual. Finally, for any v vector in \mathbb{R}^d , the product with the normal $v \cdot \mathbf{n}_0$ (respectively with the normal to the rigid foundation $v \cdot \mathbf{n}$) is denoted by $v_{\mathbf{n}_0}$ (respectively $v_{\mathbf{n}}$). Similarly, the tangential part of v is denoted by $v_{t_0} = v - v_{\mathbf{n}_0} \mathbf{n}_0$ (respectively $v_t = v - v_{\mathbf{n}} \mathbf{n}$). Since we are interested in small deformations, the body Ω is assumed to be made of a linear elastic material and we consider the small displacements assumption. Therefore, if the physical displacement is denoted by $\mathbf{u} \in \mathbf{X}$, then the stress tensor is given by Hooke's law :

$$\boldsymbol{\sigma}(\mathbf{u}) = \mathbb{C} : \boldsymbol{\epsilon}(\mathbf{u}) = 2\bar{\mu} \boldsymbol{\epsilon}(\mathbf{u}) + \bar{\lambda} \operatorname{div} \mathbf{u} \mathbf{I},$$

where $\boldsymbol{\epsilon}(\mathbf{u}) = \frac{1}{2}(\nabla \mathbf{u} + \nabla \mathbf{u}^T)$ is the linearized strain tensor, \mathbb{C} is the elasticity tensor and \mathbf{I} is the identity tensor of order 2. The coefficients $\bar{\mu}$ and $\bar{\lambda}$ (referred to as the Lamé coefficients) are such that \mathbb{C} is elliptic. Regarding external forces, the body force $\mathbf{f} \in \mathbf{L}^2(\Omega)$, and the traction (or surface load) $\boldsymbol{\tau} \in \mathbf{L}^2(\Gamma_N)$.

Remark 2. The Lamé coefficients are often expressed in terms of the Young modulus E and the Poisson coefficient ν by means of the following formulae:

$$\bar{\lambda} = \frac{E\nu}{(1+\nu)(1-2\nu)}, \quad \bar{\mu} = \frac{E}{2(1+\nu)}.$$

2.1 | Contact boundary conditions

The two essential ingredients to model the contact phenomenon are a non-penetration condition, which ensures that Ω does not penetrate Ω_{rig} , and some friction model to take into account possible frictional effects.

Non-penetration condition

At each point x of Γ_C , let us define the gap $\mathbf{g}_n(x)$, as the oriented distance function to Ω_{rig} at x , see Figure 1. The non-penetration condition can be stated as: $\mathbf{u}_n \leq \mathbf{g}_n$ a.e. on Γ_C . This condition results in two inequalities and one equality holding a.e. on the potential contact zone Γ_C :

$$\begin{cases} \mathbf{u}_n \leq \mathbf{g}_n, \\ \sigma_{\mathbf{n}_0 \mathbf{n}}(\mathbf{u}) \leq 0, \\ \sigma_{\mathbf{n}_0 \mathbf{n}}(\mathbf{u})(\mathbf{u}_n - \mathbf{g}_n) = 0, \end{cases} \quad (1)$$

where $\sigma_{\mathbf{n}_0 \mathbf{n}}(\mathbf{u}) = \sigma(\mathbf{u}) \cdot \mathbf{n}_0 \cdot \mathbf{n}$ is the normal constraint on Γ_C . Besides, we also introduce the set of admissible displacements in a standard way⁴¹:

$$\mathbf{K} := \{\mathbf{v} \in \mathbf{X} : \mathbf{v}_n \leq \mathbf{g}_n \text{ a.e. on } \Gamma_C\}.$$

Remark 3. In general, the set of boundary conditions coming from the non-penetration condition reads

$$\mathbf{u}_{\mathbf{n}_0} \leq \mathbf{g}_{\mathbf{n}_0}, \quad \sigma_{\mathbf{n}_0 \mathbf{n}_0}(\mathbf{u}) \leq 0, \quad \sigma_{\mathbf{n}_0 \mathbf{n}_0}(\mathbf{u})(\mathbf{u}_{\mathbf{n}_0} - \mathbf{g}_{\mathbf{n}_0}) = 0 \text{ on } \Gamma_C, \quad (2)$$

where $\mathbf{g}_{\mathbf{n}_0}(x)$ denotes the distance between $x \in \Gamma_C$ and the rigid foundation computed in the direction of the normal \mathbf{n}_0 to Γ_C . However, since we assume that the deformable body undergoes small displacements relatively to its reference configuration, this set of conditions is equivalent to (1). Indeed, under the small displacement hypothesis, one may replace the normal vector \mathbf{n} and the gap \mathbf{g}_n to the rigid foundation by \mathbf{n}_0 and $\mathbf{g}_{\mathbf{n}_0}$ ⁴².

In our context, we choose to write the formulation using conditions (1) instead of conditions (2). As it has been explained, this choice does not affect the solution to the contact problem. Moreover, we will see in the next sections that this slightly different formulation is very well suited to shape optimization.

Friction condition

Let $\mathfrak{F} : \Gamma_C \rightarrow \mathbb{R}$ be a uniformly Lipschitz continuous and strictly positive function representing the friction coefficient. Then the classical Coulomb friction law is expressed in the dynamic case by the following conditions on Γ_C

$$\begin{cases} |\sigma_{\mathbf{n}_0 \mathbf{t}}(\mathbf{u})| < \mathfrak{F} \sigma_{\mathbf{n}_0 \mathbf{n}}(\mathbf{u}) & \text{on } \{\dot{\mathbf{u}}_t = 0\}, \\ \sigma_{\mathbf{n}_0 \mathbf{t}}(\mathbf{u}) = -\mathfrak{F} \sigma_{\mathbf{n}_0 \mathbf{n}}(\mathbf{u}) \frac{\dot{\mathbf{u}}_t}{|\dot{\mathbf{u}}_t|} & \text{on } \{\dot{\mathbf{u}}_t \neq 0\}, \end{cases} \quad (3)$$

where $\sigma_{\mathbf{n}_0 \mathbf{t}}(\mathbf{u}) = \sigma(\mathbf{u}) \cdot \mathbf{n}_0 - \sigma_{\mathbf{n}_0 \mathbf{n}}(\mathbf{u}) \mathbf{n}$ is the tangential constraint on Γ_C , and $\dot{\mathbf{u}}_t$ denotes the sliding velocity. The sets $\{\dot{\mathbf{u}}_t = 0\}$ and $\{\dot{\mathbf{u}}_t \neq 0\}$ thus represent *sticking* and *sliding* points, respectively. When considering the static contact problem, the usual approach to approximate (3) consists in replacing the sliding velocity by a differential quotient

$$\dot{\mathbf{u}}_t \simeq \frac{\mathbf{u}_t - \mathbf{u}_t^0}{\Delta t},$$

where \mathbf{u}_t^0 is the initial value of the tangential displacement and Δt is the time step. Then, setting $\mathbf{u}_t^0 = 0$ for simplicity, we obtain the so-called *static* Coulomb friction law on Γ_C

$$\begin{cases} |\sigma_{\mathbf{n}_0 \mathbf{t}}(\mathbf{u})| < \mathfrak{F} \sigma_{\mathbf{n}_0 \mathbf{n}}(\mathbf{u}) & \text{on } \{\mathbf{u}_t = 0\}, \\ \sigma_{\mathbf{n}_0 \mathbf{t}}(\mathbf{u}) = -\mathfrak{F} \sigma_{\mathbf{n}_0 \mathbf{n}}(\mathbf{u}) \frac{\mathbf{u}_t}{|\mathbf{u}_t|} & \text{on } \{\mathbf{u}_t \neq 0\}. \end{cases} \quad (4)$$

Reusing the terminology of the dynamic case, it is common to refer to $\{\mathbf{u}_t = 0\}$ and $\{\mathbf{u}_t \neq 0\}$ as the sets of sticking and sliding points, even though this denomination is not really accurate in the static case. The static Coulomb model is the most popular among the mechanical engineering community. However, from the mathematical point of view, it is very challenging as it leads to a contact model problem under the form of a quasi-variational inequality. Existence of a solution to this variational problem is ensured only if the friction coefficient is small enough^{43,44}. As for uniqueness, partial results have been obtained^{45,46,47} but it remains an open question.

In this work, we consider a simplified version of the Coulomb model called the Tresca model or given friction model⁴⁸. Even though this simpler model is less realistic than the Coulomb friction model, it has the advantage of having nicer mathematical properties, which are extensively used in the derivation of our shape optimization algorithm¹. The principle of the Tresca model is to replace the Coulomb threshold $\sigma_{n_0 n}(\mathbf{u})$ by a fixed strictly positive function $s \in L^2(\Gamma_C)$, which leads to the following conditions on Γ_C :

$$\begin{cases} |\sigma_{n_0 t}(\mathbf{u})| < \mathfrak{F}s & \text{on } \{\mathbf{u}_t = 0\}, \\ \sigma_{n_0 t}(\mathbf{u}) = -\mathfrak{F}s \frac{\mathbf{u}_t}{|\mathbf{u}_t|} & \text{on } \{\mathbf{u}_t \neq 0\}. \end{cases} \quad (5)$$

Of course, this simplification leads to an approximate representation of frictional effects which is not correct from the mechanical point of view. For example, using the Tresca friction law, it is possible to find points that are not in contact (i.e. $\sigma_{n_0 n}(\mathbf{u}) = 0$) but that are subject to friction forces (i.e. $\sigma_{n_0 t}(\mathbf{u}) \neq 0$). Despite this non realistic representation, the Tresca model is really interesting in practice, and widely studied. Indeed, the unilateral contact problem with Coulomb friction (4) can be approximated by a fixed-point algorithm that solves at each iteration an unilateral contact problem with Tresca friction (5)^{44,49}. Therefore, the theoretical and numerical study of the Tresca problem itself often constitutes the first step towards the study of the much more cumbersome Coulomb problem.

2.2 | Mathematical formulations of the problem

Since the data has been chosen regular enough, it is known⁴⁸ that solving the contact problem with Tresca friction is equivalent to finding the displacement \mathbf{u} solution to the strong formulation:

$$-\operatorname{div} \boldsymbol{\sigma}(\mathbf{u}) = \mathbf{f} \quad \text{in } \Omega, \quad (6a)$$

$$\mathbf{u} = 0 \quad \text{on } \Gamma_D, \quad (6b)$$

$$\boldsymbol{\sigma}(\mathbf{u}) \cdot \mathbf{n}_0 = \boldsymbol{\tau} \quad \text{on } \Gamma_N, \quad (6c)$$

$$\boldsymbol{\sigma}(\mathbf{u}) \cdot \mathbf{n}_0 = 0 \quad \text{on } \Gamma, \quad (6d)$$

$$\mathbf{u}_n \leq \mathbf{g}_n, \sigma_{n_0 n}(\mathbf{u}) \leq 0, \sigma_{n_0 n}(\mathbf{u})(\mathbf{u}_n - \mathbf{g}_n) = 0 \quad \text{on } \Gamma_C, \quad (6e)$$

$$|\sigma_{n_0 t}(\mathbf{u})| < \mathfrak{F}s \quad \text{on } \{\mathbf{u}_t = 0\}, \quad (6f)$$

$$\sigma_{n_0 t}(\mathbf{u}) = -\mathfrak{F}s \frac{\mathbf{u}_t}{|\mathbf{u}_t|} \quad \text{on } \{\mathbf{u}_t \neq 0\}. \quad (6g)$$

For theoretical and numerical purposes, it is often convenient to work with a weak formulation equivalent to (6). In order to write this weak formulation, let us introduce the bilinear and linear forms $a : \mathbf{X} \times \mathbf{X} \rightarrow \mathbb{R}$ and $L : \mathbf{X} \rightarrow \mathbb{R}$, such that:

$$a(\mathbf{u}, \mathbf{v}) := \int_{\Omega} \mathbb{C} : \boldsymbol{\epsilon}(\mathbf{u}) : \boldsymbol{\epsilon}(\mathbf{v}) \, dx, \quad L(\mathbf{v}) := \int_{\Omega} \mathbf{f} \cdot \mathbf{v} \, dx + \int_{\Gamma_N} \boldsymbol{\tau} \cdot \mathbf{v} \, ds.$$

Due to the inequalities enforced on the potential contact zone Γ_C , deriving the variational formulation associated to (6) using the standard approach leads to a variational inequality (of the second kind):

$$a(\mathbf{u}, \mathbf{v} - \mathbf{u}) + j_T(\mathbf{v}) - j_T(\mathbf{u}) \geq L(\mathbf{v} - \mathbf{u}), \quad \forall \mathbf{v} \in \mathbf{K}, \quad (7)$$

where the non-linear functional $j_T : \mathbf{X} \rightarrow \mathbb{R}$ is defined by:

$$j_T(\mathbf{v}) := \int_{\Gamma_C} \mathfrak{F}s |\mathbf{v}_t| \, ds.$$

Note that this problem can also be reformulated as a minimization problem: find $\mathbf{u} \in \mathbf{K}$ solution to

$$\inf_{\mathbf{v} \in \mathbf{K}} \frac{1}{2} a(\mathbf{v}, \mathbf{v}) - L(\mathbf{v}) + j_T(\mathbf{v}). \quad (8)$$

Existence and uniqueness of the solution $\mathbf{u} \in \mathbf{K}$ have already been established, as well as equivalence between formulations (6), (7) and (8). The interested reader may find further details in the literature^{27,50,51}.

Using the tools from convex analysis and calculus of variations^{52,53}, it is possible to obtain another formulation of the contact problem based on *Lagrange multipliers*. More specifically, one can prove⁵⁴ that, if $\mathbf{u} \in \mathbf{K}$ solves (8), then there exists a unique

pair of dual variables $(\lambda, \mu) \in H^{-\frac{1}{2}}(\Gamma_C) \times \mathbf{H}^{-\frac{1}{2}}(\Gamma_C)$ such that:

$$a(\mathbf{u}, \mathbf{v}) - L(\mathbf{v}) + \langle \lambda, \mathbf{v}_n \rangle_{\Gamma_C} + \langle \mu, \mathbf{v}_t \rangle_{\Gamma_C} = 0, \quad \forall \mathbf{v} \in \mathbf{X}, \quad (9a)$$

$$\langle \lambda, \zeta \rangle_{\Gamma_C} \geq 0, \quad \forall \zeta \in H^{\frac{1}{2}}(\Gamma_C), \quad \zeta \geq 0, \quad (9b)$$

$$\langle \lambda, \mathbf{u}_n - \mathbf{g}_n \rangle_{\Gamma_C} = 0, \quad (9c)$$

$$\langle \mathfrak{F}s, |\mathbf{v}| \rangle_{\Gamma_C} - \langle \mu, \mathbf{v} \rangle_{\Gamma_C} \geq 0, \quad \forall \mathbf{v} \in \mathbf{H}^{\frac{1}{2}}(\Gamma_C), \quad (9d)$$

$$\langle \mathfrak{F}s, |\mathbf{u}_t| \rangle_{\Gamma_C} - \langle \mu, \mathbf{u}_t \rangle_{\Gamma_C} = 0. \quad (9e)$$

Furthermore, this set of equations and inequalities can be interpreted as the first order optimality conditions associated to the following saddle point problem:

$$\inf_{\mathbf{v} \in \mathbf{X}} \sup_{(\eta, \xi) \in H_+ \times \mathbf{B}_s} \mathcal{L}(\mathbf{v}, \eta, \xi), \quad (10)$$

where we have used the notations:

$$H_+ := \{ \eta \in H^{-\frac{1}{2}}(\Gamma_C) \mid \langle \eta, \zeta \rangle_{\Gamma_C} \geq 0, \forall \zeta \geq 0 \},$$

$$\mathbf{B}_s := \{ \xi \in \mathbf{H}^{-\frac{1}{2}}(\Gamma_C) \mid \langle |\xi| - \mathfrak{F}s, \mathbf{v} \rangle_{\Gamma_C} \leq 0, \forall \mathbf{v} \geq 0 \},$$

$$\mathcal{L}(\mathbf{v}, \eta, \xi) := \frac{1}{2} a(\mathbf{v}, \mathbf{v}) - L(\mathbf{v}) + \langle \eta, \mathbf{v}_n - \mathbf{g}_n \rangle_{\Gamma_C} + \langle \xi, \mathbf{v}_t \rangle_{\Gamma_C}.$$

Now that these five different formulations (6), (7), (8), (9), (10) of the original contact problem have been introduced, we are in a position to present the two regularized formulations studied in this work.

2.3 | Two regularized formulations

Even though the previous formulations of the contact problem are well understood from the mathematical point of view, their numerical resolution remains a challenging issue which constitutes an active research field. Indeed, due to the non-differentiabilities and the non-linearities involved in the problem, most of the classical numerical methods are either inapplicable or inefficient. One popular way to get around this difficulty is to consider slightly different but more regular formulations, which are easier to solve. Of course, such approximate formulations are expected to give consistent approximations of the original solution \mathbf{u} . Among all methods following this approach, we consider here the two most widely used in the industry: the *penalty method* and the *augmented Lagrangian method*. From the point of view of optimization, the main difficulties in (7) are the constraint $\mathbf{u} \in \mathbf{K}$ and the non-differentiability of j_T . In what follows, we briefly recall the two regularization procedures used by the two methods mentioned above, and we give the associated regularized formulations.

The penalty method

The penalty method was first introduced in the general case of constrained optimization⁵⁵. The idea consists in replacing the constraint by adding a penalty term to the cost functional. In this way the initial constrained optimization problem is turned into an unconstrained one. Even if this approach was being used in constrained optimization since the 1940's, its first applications to the contact problem date back to the 1980's^{56,57,58,42}. Here, the penalty approach will enable us to treat not only the constraint $\mathbf{u} \in \mathbf{K}$, but also the non-smoothness of j_T .

Let $\epsilon > 0$ be the penalty parameter. After adding a smooth penalty term j_ϵ to replace the constraint $\mathbf{u} \in \mathbf{K}$ and introducing a regularized version $j_{T,\epsilon}$ of j_T , we end up with a new minimization problem: find $\mathbf{u}_\epsilon \in \mathbf{X}$ solution to

$$\inf_{\mathbf{v} \in \mathbf{X}} \frac{1}{2} a(\mathbf{v}, \mathbf{v}) - L(\mathbf{v}) + j_{T,\epsilon}(\mathbf{v}) + j_\epsilon(\mathbf{v}). \quad (11)$$

This unconstrained differentiable optimization problem can be equivalently reformulated by means of its first order optimality condition⁵²: find $\mathbf{u}_\epsilon \in \mathbf{X}$ solution to

$$\begin{aligned} & a(\mathbf{u}_\epsilon, \mathbf{v}) - L(\mathbf{v}) + \langle j'_{T,\epsilon}(\mathbf{u}_\epsilon), \mathbf{v} \rangle + \langle j'_\epsilon(\mathbf{u}_\epsilon), \mathbf{v} \rangle = 0, \quad \forall \mathbf{v} \in \mathbf{X}, \\ \iff & a(\mathbf{u}_\epsilon, \mathbf{v}) + \frac{1}{\epsilon} (p_+ (\mathbf{u}_{\epsilon,n} - \mathbf{g}_n), \mathbf{v}_n)_{\Gamma_C} + \frac{1}{\epsilon} (\mathbf{q}(\epsilon \mathfrak{F}s, \mathbf{u}_{\epsilon,t}), \mathbf{v}_t)_{\Gamma_C} = L(\mathbf{v}), \quad \forall \mathbf{v} \in \mathbf{X}, \end{aligned} \quad (12)$$

where we have introduced the projections $p_+ : \mathbb{R} \rightarrow \mathbb{R}$ and $\mathbf{q} : \mathbb{R}_+ \times \mathbb{R}^{d-1} \rightarrow \mathbb{R}^{d-1}$ defined by: $\forall t \in \mathbb{R}$ and $\forall (\alpha, z) \in \mathbb{R}_+ \times \mathbb{R}^{d-1}$,

$$p_+(t) := \max(0, t), \quad \mathbf{q}(\alpha, z) := \begin{cases} z & \text{if } |z| \leq \alpha, \\ \alpha \frac{z}{|z|} & \text{else.} \end{cases}$$

Remark 4. These functions are indeed projections. First, p_+ is the projection onto \mathbb{R}_+ in \mathbb{R} . Then, for any fixed $\alpha \in \mathbb{R}_+$, $\mathbf{q}(\alpha, \cdot)$ represents the projection onto the ball $\mathcal{B}(0, \alpha)$ in \mathbb{R}^{d-1} .

Remark 5. The explicit expressions of j_ε and $j_{T,\varepsilon}$ are not given here since formulation (12) only requires the knowledge of their derivatives in any direction $\mathbf{v} \in \mathbf{X}$, which can be written in terms of p_+ and \mathbf{q} . The interested reader may find these expressions in the PhD thesis of the first author⁵⁹.

Let us finally state the existence, uniqueness and convergence result for the penalty formulation⁶⁰.

Theorem 1. Under our regularity assumptions on the data, there exists a unique solution $\mathbf{u}_\varepsilon \in \mathbf{X}$ to (12). Moreover, $\mathbf{u}_\varepsilon \rightarrow \mathbf{u}$ strongly in \mathbf{X} when $\varepsilon \rightarrow 0$.

The augmented Lagrangian method

Before presenting this method, we need to introduce the so-called *augmented Lagrangian formulation*. This formulation is also a regularization of the original contact problem, but contrary to the penalty formulation for which the solution $\mathbf{u}_\varepsilon \neq \mathbf{u}$ depends on ε , its solution is the same as the solution \mathbf{u} to the original formulation, no matter the value of the regularization parameter. The principle is to regularize the Lagrangian \mathcal{L} in (10) without changing its saddle-point. This leads to a set of first order optimality conditions more regular than (9). This approach was initially introduced at the end of the 1960's in the context of non-linear optimization under equality constraints^{61,62}. Then, a few decades later, it has been used to treat sliding^{57,63} and frictional^{64,65,66,67} contact problems.

Let $\gamma_1 > 0$ and $\gamma_2 > 0$ be two regularization parameters. We define the augmented Lagrangian \mathcal{L}_γ by: $\forall (\mathbf{v}, \boldsymbol{\eta}, \boldsymbol{\xi}) \in \mathbf{X} \times L^2(\Gamma_C) \times L^2(\Gamma_C)$,

$$\begin{aligned} \mathcal{L}_\gamma(\mathbf{v}, \boldsymbol{\eta}, \boldsymbol{\xi}) := & \frac{1}{2} a(\mathbf{v}, \mathbf{v}) - L(\mathbf{v}) + \frac{1}{2\gamma_1} \left(\|p_+(\boldsymbol{\eta} + \gamma_1(\mathbf{v}_n - \mathbf{g}_n))\|_{0,\Gamma_C}^2 - \|\boldsymbol{\eta}\|_{0,\Gamma_C}^2 \right) \\ & + \frac{1}{2\gamma_2} \left(\|\mathbf{q}(\mathfrak{F}s, \boldsymbol{\xi} + \gamma_2 \mathbf{v}_t)\|_{0,\Gamma_C}^2 - \|\boldsymbol{\xi}\|_{0,\Gamma_C}^2 \right), \end{aligned} \quad (13)$$

The saddle-point problem associated to this new Lagrangian is given by:

$$\inf_{\mathbf{v} \in \mathbf{X}} \sup_{(\boldsymbol{\eta}, \boldsymbol{\xi}) \in L^2 \times L^2} \mathcal{L}_\gamma(\mathbf{v}, \boldsymbol{\eta}, \boldsymbol{\xi}). \quad (14)$$

Given the expression of \mathcal{L}_γ , a necessary condition for our triplet $(\mathbf{u}, \boldsymbol{\lambda}, \boldsymbol{\mu})$ to coincide with the saddle-point of \mathcal{L}_γ is that $(\boldsymbol{\lambda}, \boldsymbol{\mu}) \in L^2(\Gamma_C) \times L^2(\Gamma_C)$. Since we have chosen the friction coefficient \mathfrak{F} regular enough and $s \in L^2(\Gamma_C)$, one can prove that the condition $\boldsymbol{\mu} \in L^2(\Gamma_C)$ is always satisfied in our context⁵⁴. However, in general, the regularity of $\boldsymbol{\lambda}$ is only $H^{-\frac{1}{2}}(\Gamma_C)$. Therefore we need to make an additional assumption in order to be able to apply our regularization procedure^{54,2}.

Assumption 1. The Lagrange multiplier $\boldsymbol{\lambda}$ belongs to $L^2(\Gamma_C)$.

With this assumption, it is now possible to show using standard techniques⁶⁸ that this augmented formulation has the desired properties. Besides, since the new saddle-point problem is posed on the vector space $\mathbf{X} \times L^2(\Gamma_C) \times L^2(\Gamma_C)$, the associated first order optimality conditions take the simpler form of equalities.

Theorem 2. Under assumption 1, for all $\gamma_1, \gamma_2 > 0$, problem (14) admits a unique solution in $\mathbf{X} \times L^2(\Gamma_C) \times L^2(\Gamma_C)$. Moreover, this solution coincides with $(\mathbf{u}, \boldsymbol{\lambda}, \boldsymbol{\mu})$ the solution to (10), and it can be fully characterized by its first order optimality conditions:

$$a(\mathbf{u}, \mathbf{v}) - L(\mathbf{v}) + (\boldsymbol{\lambda}, \mathbf{v}_n)_{\Gamma_C} + (\boldsymbol{\mu}, \mathbf{v}_t)_{\Gamma_C} = L(\mathbf{v}), \quad \forall \mathbf{v} \in \mathbf{X}, \quad (15a)$$

$$\boldsymbol{\lambda} = p_+(\boldsymbol{\lambda} + \gamma_1(\mathbf{u}_n - \mathbf{g}_n)), \quad \text{a.e. on } \Gamma_C, \quad (15b)$$

$$\boldsymbol{\mu} = \mathbf{q}(\mathfrak{F}s, \boldsymbol{\mu} + \gamma_2 \mathbf{u}_t), \quad \text{a.e. on } \Gamma_C. \quad (15c)$$

Consequently, whenever the original contact problem is regular enough (i.e. whenever Assumption 1 is satisfied), we obtain an equivalent regularized formulation which rewrites as a non-linear and non-differentiable mixed variational formulation. One possible approach to solve such a formulation is to decouple the variables using a fixed-point algorithm. This is precisely the purpose of the augmented Lagrangian algorithm. Let us briefly recall its different steps.

Algorithm 1 Augmented Lagrangian method

1. Choose $(\lambda^0, \mu^0) \in L^2(\Gamma_C) \times \mathbf{L}^2(\Gamma_C)$ and initialize $k = 0$.

2. Choose $\gamma_1^{k+1}, \gamma_2^{k+1} > 0$, then find $\mathbf{u}^{k+1} \in \mathbf{X}$ the solution to, $\forall \mathbf{v} \in \mathbf{X}$,

$$a(\mathbf{u}^{k+1}, \mathbf{v}) + (p_+(\lambda^k + \gamma_1^{k+1}(\mathbf{u}_n^{k+1} - \mathbf{g}_n)), \mathbf{v}_n)_{\Gamma_C} + (\mathbf{q}(\mathfrak{F}s, \mu^k + \gamma_2^{k+1} \mathbf{u}_t^{k+1}), \mathbf{v}_t)_{\Gamma_C} = L(\mathbf{v}). \quad (16)$$

3. Update the Lagrange multipliers:

$$\lambda^{k+1} = p_+(\lambda^k + \gamma_1^{k+1}(\mathbf{u}_n^{k+1} - \mathbf{g}_n)) \quad \text{a.e. on } \Gamma_C, \quad (17a)$$

$$\mu^{k+1} = \mathbf{q}(\mathfrak{F}s, \mu^k + \gamma_2^{k+1} \mathbf{u}_t^{k+1}) \quad \text{a.e. on } \Gamma_C. \quad (17b)$$

4. Update $k = k + 1$ and go back to step 2, until convergence.

As in the case of the penalty method, this method benefits from nice properties in terms of well-posedness and convergence⁵⁴ which are exposed in the next theorem.

Theorem 3. Let $0 < \gamma_1^1 \leq \gamma_1^2 \leq \dots$, and $0 < \gamma_2^1 \leq \gamma_2^2 \leq \dots$ be the two increasing sequences of parameters. Then for any $k \geq 1$, the iterate $\mathbf{u}^k \in \mathbf{X}$ exists and is unique. Moreover, the sequence $\{\mathbf{u}^k\}_k$ converges to \mathbf{u} strongly in \mathbf{X} , and the sequence of dual variables $\{(\lambda^k, \mu^k)\}_k$ converges to (λ, μ) weakly in $L^2(\Gamma_C) \times \mathbf{L}^2(\Gamma_C)$.

3 | SHAPE OPTIMIZATION PROBLEM

3.1 | Problem formulation

Given a cost functional $J(\Omega)$ depending explicitly on the domain Ω , and also implicitly, through $\mathbf{y}(\Omega)$ the solution to the mechanical problem on Ω , we search for a minimizer of J among the set \mathcal{U}_{ad} of admissible domains. Mathematically, the problem of minimizing J with respect to Ω or *shape optimization problem* reads:

$$\begin{aligned} \inf_{\Omega \in \mathcal{U}_{ad}} J(\Omega) &= \inf \mathcal{J}(\Omega, \mathbf{y}(\Omega)) \\ \text{subject to } &\begin{cases} \Omega \in \mathcal{U}_{ad}, \\ \mathbf{y}(\Omega) \text{ solves the contact problem}. \end{cases} \end{aligned} \quad (18)$$

Of course, here, we have $\mathbf{y}(\Omega) = \mathbf{u}_\epsilon(\Omega)$ or $\mathbf{u}^k(\Omega)$, depending on the chosen regularized formulation. Besides, we focus on rather generic cost functionals $J(\Omega)$ of type

$$J(\Omega) = \mathcal{J}(\Omega, \mathbf{y}(\Omega)) := \int_{\Omega} j(\mathbf{u}(\Omega)) \, dx + \int_{\partial\Omega} k(\mathbf{u}(\Omega)) \, ds. \quad (19)$$

The functions j, k are chosen such that they belong to $C^1(\mathbb{R}^d, \mathbb{R})$, and that their derivatives, denoted j', k' , are Lipschitz. It is also assumed that these functions and their derivatives satisfy the usual growth conditions²⁵, for all $u, v \in \mathbb{R}^d$,

$$\begin{aligned} |j(u)| &\leq C(1 + |u|^2), & |j'(u) \cdot v| &\leq C|u \cdot v|, \\ |k(u)| &\leq C(1 + |u|^2), & |k'(u) \cdot v| &\leq C|u \cdot v|, \end{aligned} \quad (20)$$

for some constants $C > 0$.

Now that J has been specified, we may turn to the set of admissible domains. Let $D \subset \mathbb{R}^d$ be a fixed bounded smooth domain, and let $\hat{\Gamma}_D \subset \partial D$ be a part of its boundary which will be the "potential" Dirichlet boundary. This means that for any domain $\Omega \subset D$, the Dirichlet boundary associated to Ω will be defined as $\Gamma_D := \partial\Omega \cap \hat{\Gamma}_D$. With these notations, we introduce the set \mathcal{U}_{ad} of all smooth open domains Ω such that the Dirichlet boundary $\Gamma_D \subset \partial D$ is of strictly positive measure, that is:

$$\mathcal{U}_{ad} := \{\Omega \subset D \mid \Omega \text{ is smooth, and } |\partial\Omega \cap \hat{\Gamma}_D| > 0\}. \quad (21)$$

3.2 | Shape sensitivity analysis

In order to build a gradient-based shape optimization algorithm, we need to compute the derivative of J with respect to the domain Ω . The notion of sensitivity with respect to the shape can be defined in several ways. In this work, we follow the method of *perturbation of the identity*^{8,13}. Let us introduce $\mathcal{C}_b^1(\mathbb{R}^d) := (\mathcal{C}^1(\mathbb{R}^d) \cap W^{1,\infty}(\mathbb{R}^d))^d$, equipped with the d -dimensional $W^{1,\infty}$ norm, denoted $\|\cdot\|_{1,\infty}$. In order to move the domain Ω , let $\theta \in \mathcal{C}_b^1(\mathbb{R}^d)$ be a (small) geometric deformation vector field. The associated perturbed or transported domain in the direction θ will be defined as: $\Omega(t) := (\text{Id} + t\theta)(\Omega)$ for any $t > 0$. With these notations, we recall the definitions of the shape derivatives of J and y at Ω in the direction θ :

$$dJ(\Omega)[\theta] := \lim_{t \searrow 0} \frac{1}{t} (J(\Omega(t)) - J(\Omega)), \quad d\mathbf{y}(\Omega)[\theta] := \lim_{t \searrow 0} \frac{1}{t} (\mathbf{y}(\Omega(t)) - \mathbf{y}(\Omega)).$$

Let us also recall that J and y are said to be *shape differentiable* if the previous limits exist for any admissible direction θ , and if the maps $\theta \mapsto dJ(\Omega)[\theta]$ and $\theta \mapsto d\mathbf{y}(\Omega)[\theta]$ are linear continuous. When there is no ambiguity, the shape derivatives of J and y at Ω in the direction θ will be simply denoted by dJ and $d\mathbf{y}$. Finally, we state a very classical result¹³ about shape differentiability of some specific functionals.

Theorem 4. Let $\psi \in W^{1,\infty}(\mathbb{R}^d) \cap W^{2,1}(\mathbb{R}^d)$, and let J_v and J_s two shape functionals defined by

$$J_v(\Omega) := \int_{\Omega} \psi(x) dx \quad \text{and} \quad J_s(\Omega) := \int_{\partial\Omega} \psi(x) ds.$$

Then J_v and J_s are shape differentiable, and their shape derivatives in any direction $\theta \in \mathcal{C}_b^1(\mathbb{R}^d)$ are given by

$$dJ_v(\Omega)[\theta] := \int_{\Omega} \psi(\theta \cdot \mathbf{n}_0) ds \quad \text{and} \quad dJ_s(\Omega)[\theta] := \int_{\partial\Omega} (\partial_{\mathbf{n}_0} \psi + \kappa \psi) (\theta \cdot \mathbf{n}_0) ds,$$

where $\kappa = \text{div}(\mathbf{n}_0)$ denotes the mean curvature of $\partial\Omega$.

Next, we will present theoretical results about shape differentiability of the solutions to the two regularized formulations (12)¹ and (15)². In practice, the augmented Lagrangian is an iterative process which will stop at some iteration k when the convergence criterion is reached. Therefore, for shape sensitivity analysis, the variational formulation considered is the one verified by the converged solution, which corresponds in this case to the formulation (15) at the last iteration k . It has already been mentioned that the variational formulations we are dealing with are not classically differentiable, therefore performing shape sensitivity analysis in this context can not be done using standard arguments. However, one can prove that these formulations are directionally differentiable. The approach followed in the two references cited above is based on this weaker notion of differentiability. In order to better understand and identify the technical difficulties we are facing, let us introduce the sets of points where non-differentiabilities occur for each formulation.

	Original	Penalty	Augmented Lagrangian
Weak contact set	$\{\mathbf{u}_n - \mathbf{g}_n = 0 \text{ and } \sigma_{\mathbf{n}_n, n}(\mathbf{u}) = 0\}$	$\{\mathbf{u}_{\varepsilon, n} - \mathbf{g}_n = 0\}$	$\{\lambda^{k-1} + \gamma_1^k (\mathbf{u}_n^k - \mathbf{g}_n) = 0\}$
Weak sticking set	$\{\mathbf{u}_t = 0 \text{ and } \sigma_{\mathbf{n}_0, t}(\mathbf{u}) = \mathfrak{F}s\}$	$\{ \mathbf{u}_{\varepsilon, t} = \varepsilon \mathfrak{F}s\}$	$\{ \boldsymbol{\mu}^{k-1} + \gamma_2^k \mathbf{u}_t^k = \mathfrak{F}s\}$

TABLE 1 Subsets of Γ_C where non-differentiabilities occur.

In Table 1, we have defined the *weak contact set* and the *weak sticking set* for the three different configurations (7), (12) and (15) following a denomination that is often used³⁴. From the mechanical point of view, these sets represent zones where changes of state occur. For instance, for the original formulation, if a point x belongs to the weak contact set, then it is in contact ($\mathbf{u}_n - \mathbf{g}_n = 0$) but there is no contact pressure ($\sigma_{\mathbf{n}_n, n}(\mathbf{u}) = 0$). Similarly, if x belongs to the weak sticking set, then is at the same time in sliding contact ($|\sigma_{\mathbf{n}_0, t}(\mathbf{u})| = \mathfrak{F}s$) and in sticking contact ($\mathbf{u}_t = 0$). From the mathematical point of view, these sets gather all points where the non-differentiabilities of \mathbf{p}_+ and \mathbf{q} are reached.

Assumption 2. The weak contact set and the weak sticking set associated to (12) and (9) are of surface measure 0.

Making this assumption enables us to prove shape differentiability^{1,2,59} of \mathbf{u}_ε and \mathbf{u}^k . Then, shape differentiability of J follows from standard arguments¹³, and we may apply Céa's method⁶⁹ to obtain an explicit expression of dJ in each case by introducing

adequate adjoint states. Before stating this result, we introduce the functions $G_+ : \mathbb{R} \rightarrow \mathcal{L}(\mathbb{R})$ and $G_s : \mathbb{R}^{d-1} \rightarrow \mathcal{L}(\mathbb{R}^{d-1})$ such that: for all $t \in \mathbb{R}$, for all $z \in \mathbb{R}^{d-1}$,

$$G_+(t) := \begin{cases} 0 & \text{if } t \leq 0, \\ 1 & \text{else,} \end{cases} \quad \text{and} \quad G_s(z) := \begin{cases} \text{Id} & \text{if } |z| \leq \mathfrak{F}s, \\ \frac{\mathfrak{F}s}{|z|} \left(\text{Id} - \frac{1}{|z|^2} z \otimes z \right) & \text{else,} \end{cases}$$

where $z \otimes z$ denotes the exterior product between z and itself, also written zz^T in the matrix representation. These functions, which are generalized derivatives⁷⁰ of p_+ and \mathbf{q} , will be useful to write the adjoint variational formulations. Another quantity of interest is the linear form L_{adj} , which depends only on J and \mathbf{y} :

$$L_{adj}[\mathbf{y}](\mathbf{v}) = - \int_{\Omega} j'(\mathbf{y}) \cdot \mathbf{v} \, dx - \int_{\partial\Omega} k'(\mathbf{y}) \cdot \mathbf{v} \, ds, \quad \forall \mathbf{v} \in \mathbf{X}. \quad (22)$$

With these notations, we can define the adjoint states \mathbf{p}_ϵ and \mathbf{p}^k in \mathbf{X} such that:

$$a(\mathbf{p}_\epsilon, \mathbf{v}) + \frac{1}{\epsilon} (G_+(\mathbf{u}_{\epsilon,n} - \mathbf{g}_n) \mathbf{p}_{\epsilon,n}, \mathbf{v}_n)_{\Gamma_C} + \frac{1}{\epsilon} (G_{\epsilon s}(\mathbf{u}_{\epsilon,t}) \mathbf{p}_{\epsilon,t}, \mathbf{v}_t)_{\Gamma_C} = L_{adj}[\mathbf{u}_\epsilon](\mathbf{v}), \quad \forall \mathbf{v} \in \mathbf{X}, \quad (23a)$$

$$a(\mathbf{p}^k, \mathbf{v}) + \gamma_1^k (G_+(\lambda^{k-1} + \gamma_1^k (\mathbf{u}_n^k - \mathbf{g}_n)) \mathbf{p}_n^k, \mathbf{v}_n)_{\Gamma_C} + \gamma_2^k (G_s(\mu^{k-1} + \gamma_2^k \mathbf{u}_t^k) \mathbf{p}_t^k, \mathbf{v}_t)_{\Gamma_C} = L_{adj}[\mathbf{u}^k](\mathbf{v}), \quad \forall \mathbf{v} \in \mathbf{X}. \quad (23b)$$

Lemma 1. For any $\epsilon > 0$ and any $k \geq 1$, the solutions \mathbf{p}_ϵ and \mathbf{p}^k to the two formulations in (23) exist and are unique in \mathbf{X} .

Proof. Since we are dealing with linear variational formulations posed on the Hilbert space \mathbf{X} , we can apply Lax-Milgram lemma. Let us start with the penalty adjoint formulation. First, it is clear that $L_{adj}[\mathbf{u}_\epsilon]$ is linear and continuous on \mathbf{X} due to the growth assumptions (20). Besides the left hand-side is a bilinear form on $\mathbf{X} \times \mathbf{X}$. Then, using the expressions of G_+ and G_s , Cauchy-Schwarz inequality and the trace theorem, one gets that for all $(\mathbf{w}, \mathbf{v}) \in \mathbf{X} \times \mathbf{X}$,

$$\begin{aligned} \left| (G_+(\mathbf{u}_{\epsilon,n} - \mathbf{g}_n) \mathbf{w}_n, \mathbf{v}_n)_{\Gamma_C} \right| &\leq (|\mathbf{w}_n|, |\mathbf{v}_n|)_{\Gamma_C} \leq C \|\mathbf{w}\|_{\mathbf{X}} \|\mathbf{v}\|_{\mathbf{X}}, \\ \left| (G_{\epsilon s}(\mathbf{u}_{\epsilon,t}) \mathbf{w}_t, \mathbf{v}_t)_{\Gamma_C} \right| &\leq (|\mathbf{w}_t|, |\mathbf{v}_t|)_{\Gamma_C} \leq C \|\mathbf{w}\|_{\mathbf{X}} \|\mathbf{v}\|_{\mathbf{X}}. \end{aligned}$$

Finally, we notice that for all $t \in \mathbb{R}$, $z \in \mathbb{R}^{d-1}$, the functions $G_+(t)$ and $G_s(z)$ verify:

$$G_+(t)y \cdot y \geq 0, \quad \forall y \in \mathbb{R}, \quad \text{and} \quad G_s(z)h \cdot h \geq 0, \quad \forall h \in \mathbb{R}^{d-1}.$$

Therefore, it follows from the coercivity of a that the left hand-side of the formulation is also a coercive bilinear form. Lax-Milgram lemma enables us to conclude that $\mathbf{p}_\epsilon \in \mathbf{X}$ exists and is unique. The proof for \mathbf{p}^k can be done using exactly the same arguments. \square

Theorem 5. Under Assumption 2, the solutions \mathbf{u}_ϵ and \mathbf{u}^k to (12) and (15) are shape differentiable. Thus the cost functional J is also shape differentiable in these cases. Moreover, when $\mathbf{u}_\epsilon, \mathbf{u}^k, \mathbf{p}_\epsilon, \mathbf{p}^k \in \mathbf{H}^2(\Omega) \cap \mathbf{X}$, the shape derivative of J in any direction $\theta \in \mathcal{C}_b^1(\mathbb{R}^d)$ is given by

$$dJ(\Omega)[\theta] = \int_{\partial\Omega} \mathbf{g}(\theta \cdot \mathbf{n}_0) \, ds.$$

with $\mathbf{g} = \mathbf{g}_\epsilon$ or \mathbf{g}^k depending on the formulation considered. More specifically, one has

$$\begin{aligned} \mathbf{g}_\epsilon &= j(\mathbf{u}_\epsilon) + \mathbb{C} : \boldsymbol{\epsilon}(\mathbf{u}_\epsilon) : \boldsymbol{\epsilon}(\mathbf{p}_\epsilon) - \mathbf{f} \mathbf{p}_\epsilon + \chi_{\Gamma_N}(\kappa + \partial_{\mathbf{n}_0}) (k(\mathbf{u}_\epsilon) - \boldsymbol{\tau} \mathbf{p}_\epsilon) \\ &\quad + \frac{1}{\epsilon} \chi_{\Gamma_C}(\kappa + \partial_{\mathbf{n}_0}) (p_+(\mathbf{u}_{\epsilon,n} - \mathbf{g}_n) \mathbf{p}_{\epsilon,n} + \mathbf{q}(\epsilon \mathfrak{F}s, \mathbf{u}_{\epsilon,t}) \mathbf{p}_{\epsilon,t}), \\ \mathbf{g}^k &= j(\mathbf{u}^k) + \mathbb{C} : \boldsymbol{\epsilon}(\mathbf{u}^k) : \boldsymbol{\epsilon}(\mathbf{p}^k) - \mathbf{f} \mathbf{p}^k + \chi_{\Gamma_N}(\kappa + \partial_{\mathbf{n}_0}) (k(\mathbf{u}^k) - \boldsymbol{\tau} \mathbf{p}^k) \\ &\quad + \chi_{\Gamma_C}(\kappa + \partial_{\mathbf{n}_0}) (\lambda^k \mathbf{p}_n^k + \boldsymbol{\mu}^k \mathbf{p}_t^k), \end{aligned}$$

where χ_{Γ_N} and χ_{Γ_C} represent the characteristic functions of Γ_N and Γ_C .

Proof. The result about shape differentiability of \mathbf{u}_ϵ and \mathbf{u}^k has been obtained in previous works^{1,2}. The reader is referred to these references for the detailed proof of this part of the theorem.

Now, the shape differentiability property for these solutions enables us to apply Céa's method to get an expression of dJ . As in the proof of Lemma 1, since both formulations are very similar in terms of technical difficulties, we focus on the (formal)

proof in the case of the penalty method, and leave the case of the augmented Lagrangian method to the reader. Let us first define the Lagrangian \mathcal{L}_ϵ by, for all $(\Omega, \mathbf{v}, \mathbf{w}) \in \mathcal{U}_{ad} \times \mathbf{X} \times \mathbf{X}$,

$$\begin{aligned}\mathcal{L}_\epsilon(\Omega, \mathbf{v}, \mathbf{w}) &:= a(\mathbf{v}, \mathbf{w}) + \frac{1}{\epsilon} (\mathbf{p}_+ (\mathbf{v}_n - \mathbf{g}_n), \mathbf{w}_n)_{\Gamma_C} + \frac{1}{\epsilon} (\mathbf{q}(\epsilon \mathfrak{F}s, \mathbf{v}_t), \mathbf{w}_t)_{\Gamma_C} - L(\mathbf{w}) + \mathcal{J}(\Omega, \mathbf{v}) \\ &= \int_{\Omega} \mathbb{C} : \boldsymbol{\epsilon}(\mathbf{v}) : \boldsymbol{\epsilon}(\mathbf{w}) dx + \frac{1}{\epsilon} \int_{\Gamma_C} \mathbf{p}_+ (\mathbf{v}_n - \mathbf{g}_n) \mathbf{w}_n ds + \frac{1}{\epsilon} \int_{\Gamma_C} \mathbf{q}(\epsilon \mathfrak{F}s, \mathbf{v}_t) \mathbf{w}_t ds \\ &\quad - \int_{\Omega} \mathbf{f} \mathbf{w} dx - \int_{\Gamma_N} \boldsymbol{\tau} \mathbf{w} ds + \int_{\Omega} j(\mathbf{v}) dx + \int_{\partial\Omega} k(\mathbf{v}) ds.\end{aligned}$$

Note that, given this definition, the following equality holds for all $\mathbf{w} \in \mathbf{X}$,

$$J(\Omega) = \mathcal{J}(\Omega, \mathbf{u}_\epsilon(\Omega)) = \mathcal{L}_\epsilon(\Omega, \mathbf{u}_\epsilon(\Omega), \mathbf{w}).$$

Differentiating this relation with respect to the shape gives us an expression of the shape derivative of J , valid for any $\mathbf{w} \in \mathbf{X}$:

$$\begin{aligned}dJ(\Omega)[\theta] &= \left\langle \frac{d}{d\Omega} (\mathcal{L}_\epsilon(\Omega, \mathbf{u}_\epsilon(\Omega), \mathbf{w})) ; \theta \right\rangle \\ &= \left\langle \frac{\partial \mathcal{L}_\epsilon}{\partial \Omega}(\Omega, \mathbf{u}_\epsilon, \mathbf{w}); \theta \right\rangle + \left\langle \frac{\partial \mathcal{L}_\epsilon}{\partial \mathbf{v}}(\Omega, \mathbf{u}_\epsilon, \mathbf{w}); d \mathbf{u}_\epsilon \right\rangle.\end{aligned}$$

It is possible to cancel the second term in the last expression by taking $\mathbf{w} = \mathbf{p}_\epsilon$. Indeed, with this specific choice, this term is equal to the variational formulation (23) with test-function $\mathbf{v} = d \mathbf{u}_\epsilon$. Therefore one finally gets

$$dJ(\Omega)[\theta] = \left\langle \frac{\partial \mathcal{L}_\epsilon}{\partial \Omega}(\Omega, \mathbf{u}_\epsilon, \mathbf{p}_\epsilon); \theta \right\rangle,$$

which leads to the desired formula after application of Theorem 4. \square

Remark 6. For example, Assumption 2 is satisfied when all weak contact points and all weak sticking points represent a finite number of points in 2D or a finite number of curves in 3D.

Remark 7. The fact that dJ depends only on the normal component $\theta \cdot \mathbf{n}_0$ of θ on the boundary $\partial\Omega$ is not specific to our context. It is actually a consequence of the Hadamard-Zolésio structure theorem¹¹.

Now that we have obtained expressions of the shape derivatives of J for our two regularized problems which are rather easy to compute in practice, we can build our gradient-based shape optimization algorithm.

4 | DESCRIPTION OF THE ALGORITHM

Let us first recall that we aim at solving the shape optimization problem:

$$\inf_{\Omega \in \mathcal{U}_{ad}} J(\Omega),$$

where J is a functional of type (19), Ω is the domain on which the contact problem is posed, and \mathcal{U}_{ad} is the set of admissible shapes, as defined in (21). In order to solve this problem numerically, we propose a gradient-based optimization algorithm which generates a sequence of shapes $\{\Omega^l\}_l$ such that the monotonicity of J is ensured. In other words, the generated sequence of shapes is such that $J(\Omega^{l+1}) < J(\Omega^l)$ for each l . Here is a brief presentation of the different steps of the algorithm.

Remark 8. In practice, at the beginning of the iterative process, it might be useful to accept shapes Ω^{l+1} such that $J(\Omega^{l+1}) < \beta J(\Omega^l)$, with $\beta > 1$. This prevents the algorithm from falling too fast in the neighbourhood of a local minimum.

The goal of this section is to describe the body of the algorithm, namely steps 2, 3, 4 and 5. In these descriptions, we will omit the superscript l related to the current iteration for the reader's convenience. For example, the variables Ω^l, θ^l will be replaced by Ω, θ . Besides, since the domains considered are represented by means of a level-set function, we begin with a short and very formal presentation of the level-set method in the context of shape optimization.

Algorithm 2 Shape optimization algorithm

1. Choose a domain Ω^0 and initialize $l = 0$.
 2. Solve the primal formulation (12) or (15) in Ω^l .
 3. Solve the adjoint formulation (23a) or (23b) in Ω^l .
 4. Find a descent direction θ^l .
 5. Update the domain $\Omega^l \rightarrow \Omega^{l+1}$.
 6. Update $l = l + 1$ and go back to step 2, until convergence is reached.
-

4.1 | Level-set representation of shapes

The level-set method was first introduced by Osher and Sethian⁷¹ to give an implicit representation of the boundary of a smooth domain $\Omega \subset \mathbb{R}^d$. More specifically, Ω is associated to the set of negative values of an auxiliary function ϕ defined on the whole space \mathbb{R}^d (in practice, ϕ is defined on a computational domain D assumed to be large enough). Similarly, the boundary $\partial\Omega$ is defined as the zero level-set of ϕ . In other words, ϕ satisfies:

$$\begin{cases} \phi(x) < 0 & \text{if } x \in \Omega, \\ \phi(x) = 0 & \text{if } x \in \partial\Omega, \\ \phi(x) > 0 & \text{if } x \in D \setminus \overline{\Omega}. \end{cases} \quad (24)$$

A typical choice of function ϕ is the signed distance function¹² to $\partial\Omega$. One of the main advantages of this method is that it enables us to represent a domain $\Omega(t)$ which evolves during a time interval $[0, T]$ under the action of a velocity field θ . Indeed, it suffices to consider a function ϕ depending on both space and time, i.e. for all $t \in [0, T]$, $\phi(t, \cdot)$ is the level-set function associated to $\Omega(t)$. Let us assume that we start with a domain $\Omega(0) = \Omega^0$, represented by some function ϕ^0 . Then the evolution of Ω with respect to t can be modeled by the following partial differential equation on $[0, T] \times \mathbb{R}^d$ (referred to as the *level-set advection equation*), associated with a suitable initial condition,

$$\begin{aligned} \frac{\partial \phi}{\partial t}(t, x) + \theta(t, x) \cdot \nabla \phi(t, x) &= 0, \\ \phi(0, x) &= \phi^0(x). \end{aligned} \quad (25)$$

Moreover, if we choose a velocity field θ directed along the direction of the normal \mathbf{n}_o (as suggested by the result of Theorem 5), say $\theta = \theta \mathbf{n}_o$, then (25) can be rewritten as:

$$\begin{aligned} \frac{\partial \phi}{\partial t}(t, x) + \theta(t, x) \cdot |\nabla \phi(t, x)| &= 0, \\ \phi(0, x) &= \phi^0(x), \end{aligned} \quad (26)$$

which is now a *Hamilton-Jacobi equation*.

The nice properties of this method have made it very popular in the context of shape optimization since its first developments in the beginning of the 2000's^{72,5}. Compared to approaches based on an explicit and fully discrete representation of the shape, the level-set approach is an interesting alternative as it gives a continuous and smooth (albeit implicit) representation of the shape all along the geometric deformation process. Furthermore, it is also naturally well suited to deal with changes of topology¹⁸.

4.2 | Resolution of the primal formulation

Let D_h be the discretization of the domain D , where h stands for the mesh size. As it will be seen in details in subsection 4.5, at each iteration of Algorithm 2, our cutting/remeshing procedure provides us with a discretized version Ω_h of Ω as a subdomain of D_h . This subdomain Ω_h is our computational domain for the resolution of the contact problem. In order to maximize the efficiency of this cutting/remeshing procedure, we consider unstructured meshes made of triangles in 2D and tetrahedra in 3D. This enables us to use standard Lagrange finite elements (typically P^1 or P^2) to discretize our variables.

Case of the penalty method.

We choose a discretization $\mathbf{u}_{\varepsilon,h} \in P^2$ of \mathbf{u}_ε , for which the convergence analysis has been established⁶⁰. Since the continuous problem (12) is non-linear and non-differentiable, we solve it using a semi-smooth Newton method⁷⁰.

Case of the augmented Lagrangian method.

In this case, we choose a discretization $\mathbf{u}_h^k \in P^2$ of \mathbf{u}^k and $(\lambda_h^k, \mu_h^k) \in P^1 \times P^1$ of (λ^k, μ^k) . The convergence analysis has already been performed⁷³ for such a discretization of (15). Note that the augmented Lagrangian method can also be understood as a special case of Nitsche's method, for which the convergence analysis has also been established^{40,74}. As in the case of the penalty method, we use a semi-smooth Newton approach.

4.3 | Resolution of the adjoint formulation

Given that the adjoint state lies in the same Sobolev space as the primal state, we use the same discretization for both of them, namely P^2 . Then, we recall that unlike the primal formulation, the adjoint formulation is linear, which makes it easier to solve. The right hand-side is given by (22) and can be easily assembled using the primal state $\mathbf{u}_{\varepsilon,h}$ or \mathbf{u}_h^k that has just been computed. As far as the left hand-side is concerned, let us first notice that the adjoint formulation (23) is obtained by differentiating the primal formulation with respect to the state variable. Consequently, in order to build the algebraic system solved by $\mathbf{p}_{\varepsilon,h}$ (or \mathbf{p}_h^k), we may reuse the matrix from the last Newton iteration that led to $\mathbf{u}_{\varepsilon,h}$ (or \mathbf{u}_h^k).

Remark 9. In practice, computing the adjoint state is not very costly as it is similar to one Newton iteration in terms of complexity. Here, it is even less costly since the assembly and the *LU* factorization of the matrix have already been performed.

4.4 | Computation of a descent direction

Given that the evolution of the shape is simulated by solving (26), we need the vector field $\theta = \theta \mathbf{n}_0$ to be defined on the whole computational domain D . This vector field is also expected to be a descent direction, i.e. it must satisfy $dJ(\Omega)[\theta] < 0$. A rather common choice^{75,5} consists in taking $\theta \in H^1(D)$ solution to:

$$\int_D \nabla \theta \cdot \nabla v + \alpha \theta v \, dx = -dJ(\Omega)[v \mathbf{n}_0] = - \int_{\partial\Omega} g v \, ds, \quad \forall v \in H^1(D), \quad (27)$$

where the parameter $\alpha > 0$ is usually of the same order of magnitude as the mesh size h ⁷⁶, and $g = g_e$ or g^k depending on the formulation considered (cf Theorem 5). Obviously, such a choice ensures that θ is a descent direction. Besides, formulation (27) can be discretized using standard Lagrange finite elements, e.g. $\theta_h \in P^1$ or P^2 in D_h .

4.5 | Domain evolution

In order to find the new (perturbed) domain given a vector field $\theta = \theta \mathbf{n}_0$ computed at the previous step, we aim at solving (26) on a time interval $[0, T]$ taking $\theta(t, x) = \theta(x)$ in $[0, T] \times D$. In this work, this equation is solved using finite differences (in time and space) on an auxiliary cartesian grid. There are two main motivations for this choice. The first one is essentially practical: the numerical resolution of (26) on a cartesian grid using the fast-marching method^{77,78} is efficient, easy to implement and extremely robust, which is an essential feature when solving a shape optimization problem. Second, having two different meshes for the level-set equation and the mechanical problem enable us to work with a very fine cartesian grid, which gives us a very accurate and smooth representation of the shape, without increasing the computational cost related to solving the contact problem. This can be interpreted as a two-level approach: the representation of the shape (low computational cost) is considered at a fine level and the mechanical quantities as well as the shape gradients (high computational cost) are considered at a coarse level.

In practice, we take ϕ as the signed distance function to $\partial\Omega$. Then, given a grid D_Δ of D consisting of the nodes (x_i, y_j, z_k) , we get a discrete $\phi_{ijk}^n = \phi(t^n, (x_i, y_j, z_k))$ on D_Δ for each $n \in \{0, \dots, N\}$, where $t^0 = 0$ and $t^N = T$. After evaluating the descent direction θ_h defined in D_h at each grid point of D_Δ , we end up with θ_{ijk} defined on D_Δ . Now, taking ϕ_{ijk}^0 as the signed distance computed at the last step t^N of the previous shape optimization iteration, we solve (26) and obtain ϕ_{ijk}^N , the representation of the new domain after evolution. Finally, projecting this result onto the finite element mesh by means of a L^2 -projection yields an implicit representation of the new shape on D_h , denoted by $\phi_h \in P^m$, $m \geq 1$.

Remark 10. Even if ϕ^0 is very smooth and represents a distance function, there is no guarantee that these nice properties still hold at each step of the numerical resolution of (26). In practice, the solution may become irregular, especially in the neighbourhood of $\{\phi = 0\}$. It is also possible that at some point, one gets $|\nabla\phi| \ll 1$ ou $\gg 1$, which would mean that ϕ is no longer a good approximation of a distance function. In order to avoid these issues, one may periodically *reinitialize* during the resolution of (26). More specifically, for some fixed $\bar{t} \in [0, T]$, reinitializing $\bar{\phi} = \phi(\bar{t}, \cdot)$ consists in replacing $\bar{\phi}$ by the solution ψ to:

$$\begin{cases} \partial_t \psi + \operatorname{sgn}(\bar{\phi})(|\nabla \psi| - 1) = 0 & \text{in } [0, +\infty) \times D, \\ \psi(0, x) = \bar{\phi}(x) & \text{in } D. \end{cases} \quad (28)$$

Since (28) is a Hamilton-Jacobi equation, we may use the same numerical scheme as before to solve it.

Building Ω_h .

At this stage, we would like to decide whether the new shape is accepted or rejected. Thus we should be able to check if it satisfies the geometric criteria necessary to belong to \mathcal{U}_{ad} , and we should be able to compute $J(\Omega_h)$. From the point of view of a conformal discretization approach, this means that the discrete domain Ω_h has to be constructed. Since we know ϕ_h on D_h , we can compute the intersection between the coarse level boundary $\{\phi_h = 0\}$ and the edges of D_h . Then, it suffices to add the nodes corresponding to these intersections to D_h , as well as all other necessary mesh components (edges, faces, elements) necessary to ensure the validity of the new mesh. We end up with a new mesh \tilde{D}_h of D that contains a submesh Ω_h representing the new domain.

This approach simply consists in *cutting* the mesh around the coarse level-set $\{\phi_h = 0\}$, and it is not new⁷⁹ in the case of a field $\phi_h \in P^1$. It has also been used in the context of shape optimization^{24,80,25} as the preliminary step of a more sophisticated remeshing procedure. This method has two main advantages: it is easy to implement, and robust. Nevertheless, it may generate meshes with low quality elements (stretched, potentially very small) and the interface $\partial\Omega_h$ might be irregular, especially in 3D.

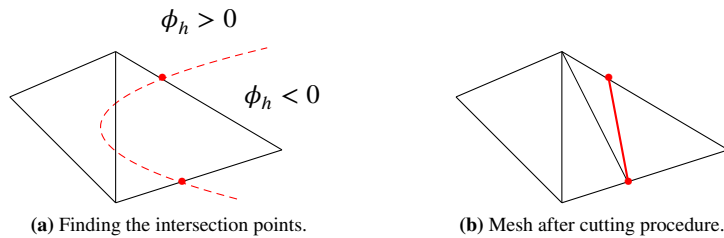


FIGURE 2 Mesh-cutting procedure for $\phi_h \in P^1$.

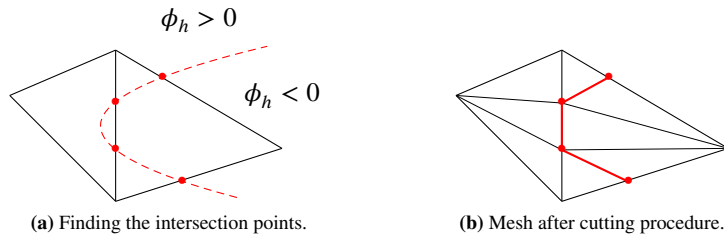


FIGURE 3 Mesh-cutting procedure for $\phi_h \in P^2$.

In this work, we choose to follow this approach despite its drawbacks, but we propose to increase its accuracy by considering a field $\phi_h \in P^m$ with $m > 1$. This enables us to find a greater number of intersection points between the level set $\{\phi_h = 0\}$ and D_h , and it leads to a more accurate representation of the underlying smooth boundary $\{\phi = 0\}$. As illustrated in Figure 2 and

Figure 3, using a P^2 interpolation instead of a P^1 interpolation for ϕ_h really seems to make a difference in terms of accuracy, even in rather simple 2D cases.

Example

Let us consider a three-dimensional example in order to illustrate the influence of the interpolation degree of ϕ_h on Ω_h . The discrete computational domain D_h consists in a regular mesh of the cube $D = [0, 1]^3$ consisting in 4913 vertices, see Figure 5a. Let us define the scalar polynomial function of degree 4

$$\phi(x) := 16 \left(x - \frac{1}{2} \right)^4 + \left(y - \frac{1}{2} \right)^2 + \left(z - \frac{1}{2} \right)^2 - \frac{1}{4}.$$

In Figure 4, we have displayed the result after performing our mesh-cutting procedure in the three different cases $\phi_h \in P^1$, P^2 and P^3 . As expected, the surfaces $\{\phi_h = 0\}$ obtained when using P^2 and P^3 interpolations are smoother, for a similar

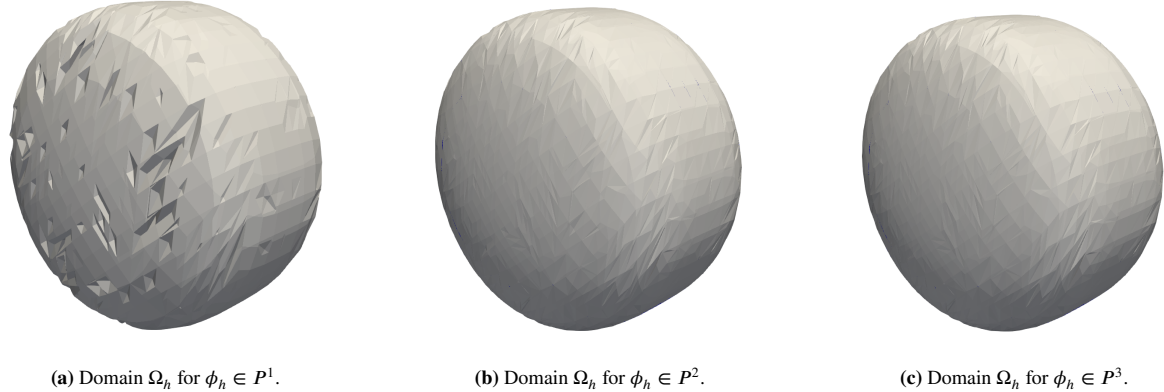


FIGURE 4 Domains Ω_h after cutting the mesh around the surface $\{\phi_h = 0\}$.

number of additional vertices: 3563 in the P^1 case, 3574 in the P^2 case and 3579 in the P^3 case. However, there is no significant improvement when using a cubic interpolation compared to a quadratic one.

In practice, the observations made in this example remain true in most cases. Therefore, we choose to work with $\phi_h \in P^2$, which in our context appears to be the best compromise. Besides, as it can be seen in Figure 5, the choice of interpolation degree does not seem to influence the quality of the resulting mesh.

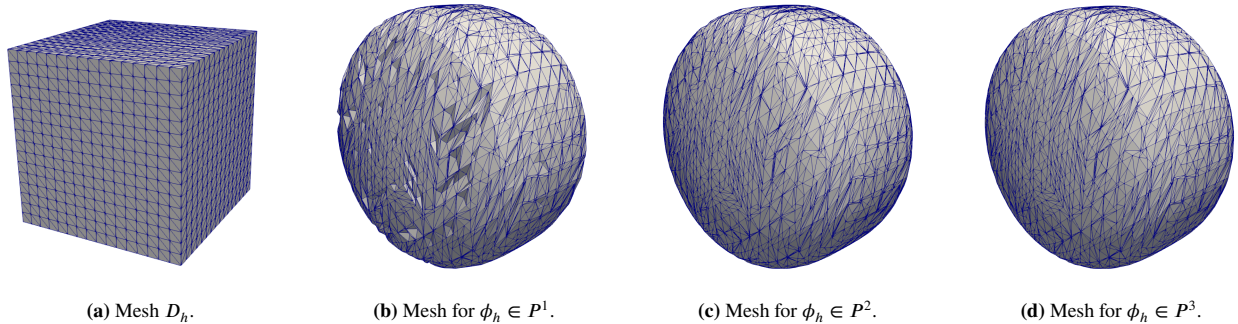


FIGURE 5 Meshes after cutting procedure around the surface $\{\phi_h = 0\}$.

Remark 11. In the previous example, we see that the resulting surface mesh of $\{\phi_h = 0\}$ contains very small and stretched elements. This could be an obstacle for the numerical resolution when the problem considered is particularly difficult to solve (large number of unknowns, strong non-linearities, etc). In this work, we restrict ourselves to the case of linearized elasticity, on meshes containing at most 5000 vertices. Therefore we do not encounter such difficulties when solving the mechanical problem on these meshes. Moreover, even if something wrong happened at some iteration, the shape optimization process would not be jeopardized thanks to the robustness of the optimization solver. Nevertheless, in order to extend our shape optimization method to industrial benchmarks (fine meshes, complex geometries) in the case of contact with Coulomb friction and non-linear elastic materials, it would be necessary to add a step that improves the quality of the mesh. An idea would be to control the quality of the mesh, then perform a complete or partial mesh adaptation procedure⁷⁶.

5 | NUMERICAL RESULTS

In this section, we present numerical results obtained when applying our shape optimization algorithm to some benchmarks in two and three dimensions. More specifically, we get interested in two types of configurations. First, in order to validate our approach, we apply our algorithm in a specific configuration coming from the literature^{81,36} where the contact zone is known a priori. In this configuration, we fix a set of zones $\hat{\Gamma}_C \subset \partial D$ where contact phenomena may occur. Then, during the optimization process, the potential contact zone Γ_C associated to a given shape Ω will be defined as $\Gamma_C := \hat{\Gamma}_C \cap \partial\Omega$. This means that the treatment of Γ_C is similar to the one of Γ_D : if the shape "holds on" to a part of $\hat{\Gamma}_C$, then there will be contact in this zone, otherwise the boundary is free of constraint. Especially, no shape derivative needs to be computed on Γ_C in this case. Second, we consider configurations where the contact zone is not known a priori. We only define a rigid body Ω_{rig} such that the deformable body might come in contact with Ω_{rig} under the action of external forces and surface loads. Then, given a shape Ω , the computation of the gap will enable us to determine which points come in contact with Ω_{rig} among the set of all points $\partial\Omega \setminus (\Gamma_D \cup \Gamma_N)$. In this more general configuration, we may use the shape derivative on Γ_C to also optimize this part of the boundary without enforcing any a priori constraint. To the best of our knowledge, there does not exist any three-dimensional benchmark in the literature for such configurations in the case of non planar rigid bodies. Therefore we propose a new one which is inspired by a two-dimensional benchmark³⁸.

The algorithm has been implemented in MEF++, the finite element based multiphysics platform developed at the GIREF (*Groupe Interdisciplinaire de Recherche en Éléments Finis*, at Laval University). The interested reader is referred to the website <https://giref.ulaval.ca/> for further information about this research code.

In what follows, we always consider isotropic linear elastic materials with Young modulus $E = 1$ and Poisson coefficient $\nu = 0.3$. Besides, as it is often the case in structural optimization, the cost functional J is defined as a linear combination of the volume Vol and the compliance C :

$$J(\Omega) := \alpha_1 C(\Omega) + \alpha_2 Vol(\Omega) = \int_{\Omega} (\alpha_1 \mathbf{f} \cdot \mathbf{y}(\Omega) + \alpha_2) dx + \int_{\Gamma_N} \alpha_1 \boldsymbol{\tau} \cdot \mathbf{y}(\Omega) ds,$$

where α_1 and α_2 are real positive coefficients and $\mathbf{y} = \mathbf{u}_e$ or \mathbf{u}^k depending on the formulation solved.

Remark 12. As it has been mentioned before, the level-set method is well-suited to treat changes of topology, especially to close or merge "holes" (i.e. connected components of $D \setminus \Omega$). Therefore, a common practice^{5,18} consists in taking an initial shape Ω^0 containing holes. This can be seen as a way to enlarge the set of admissible shapes used in practice.

5.1 | Example where the contact zone is known a priori

Two-dimensional bridge.

This first benchmark comes from the literature⁸². In this reference, the authors solve a classically differentiable contact formulation obtained using the penalty method with an additional regularization step. Their representation of the shapes is also based on the level-set method, but they do not have a mesh Ω_h . Instead, the boundary conditions are imposed weakly on $\partial\Omega \setminus D$. Due to the similarities between their method and ours, it is interesting to tackle this benchmark and compare our result to theirs in order to validate our algorithm. The computational domain is given by $D = [0, 1] \times [0, 1]$. Two disjoint potential contact zones are placed at the bottom-left and bottom-right parts of ∂D , and a Neumann boundary condition is enforced at the bottom-center of ∂D , see Figure 6a. As for physical forces, we set $\mathbf{f} = 0$ and $\boldsymbol{\tau} = (0, -0.01)$. The coefficients in the expression of J satisfy

$\alpha_1 = 25$, $\alpha_2 = 0.01$. In the case of the penalty method, the penalty parameter is such that $\varepsilon = 10^8$, and in the case of the augmented Lagrangian method, we take $\gamma_1^k = \gamma_2^k = 1000$ for all k . Finally, in the frictional case, the Tresca threshold is set to $s = 10^{-2}$ (order of magnitude of the normal constraint $\sigma_{n_0 n}$), and the friction coefficient is $\mathfrak{F} = 0.2$. The optimal designs obtained in each case are displayed in Figure 6.

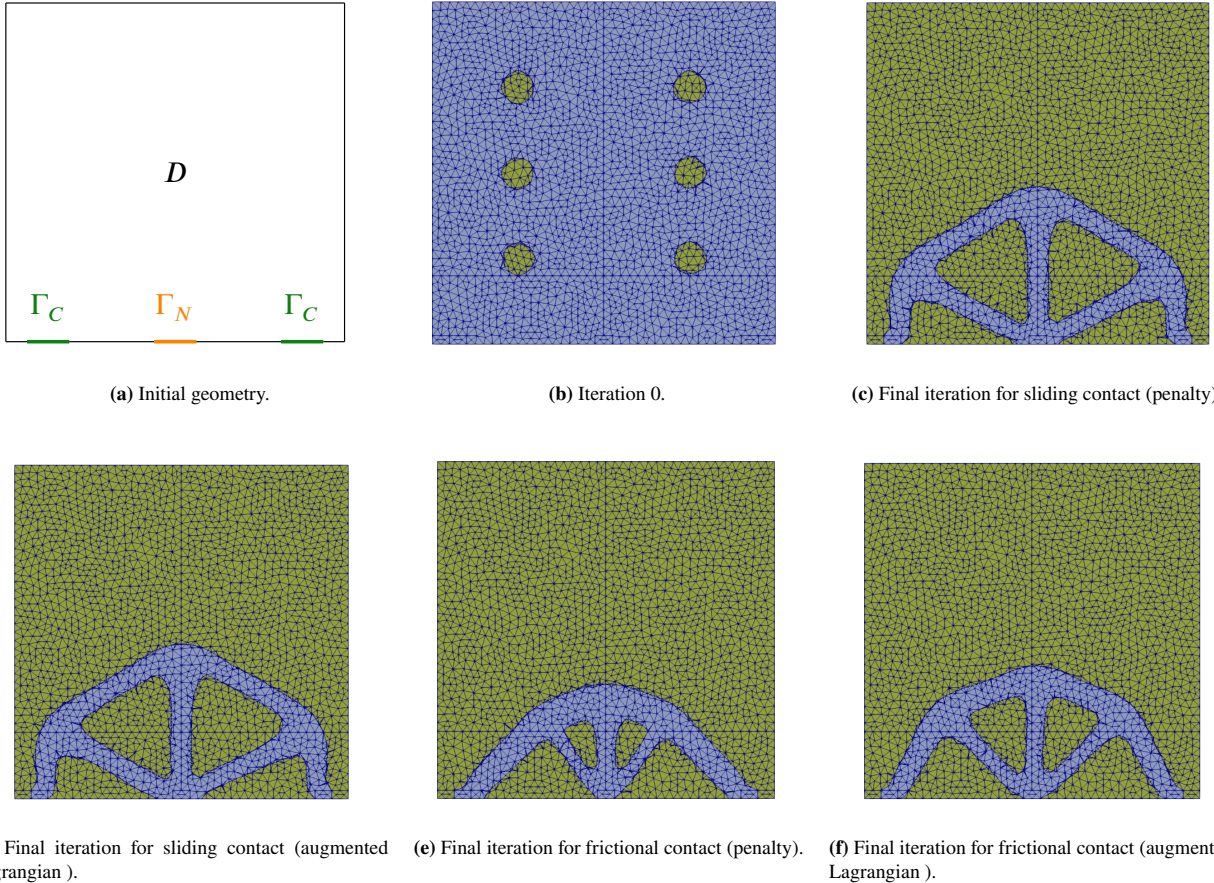


FIGURE 6 Initial and final designs for the 2D bridge (Ω_h in blue, $D_h \setminus \Omega_h$ in yellow).

In the case of sliding contact, the optimal designs obtained for both formulation (penalty and augmented Lagrangian) are very similar. They are also very close to the solution obtained in the work mentioned above³⁶. Especially, we note that the legs of the bridge are vertical above the contact zone, this limitates sliding and improves the rigidity of the structure. The convergence curves of $J(\Omega^l)$, plotted in Figure 7, also have similar behaviours for the two formumations, and they seem to converge to the same value. However, in the frictional case, the optimal designs look quite different for the two formulations, but the values of J are very close, see Figure 7. We still obtain shapes with properties similar to the one in the reference. As expected, thanks to the friction, the legs of the bridge may incline without deteriorating the rigidity of the structure.

5.2 | Examples where the contact zone is not known a priori

In order to study the validity of the results from Theorem 5 in numerical practice, we consider a case which tests the shape derivatives on the contact zone.

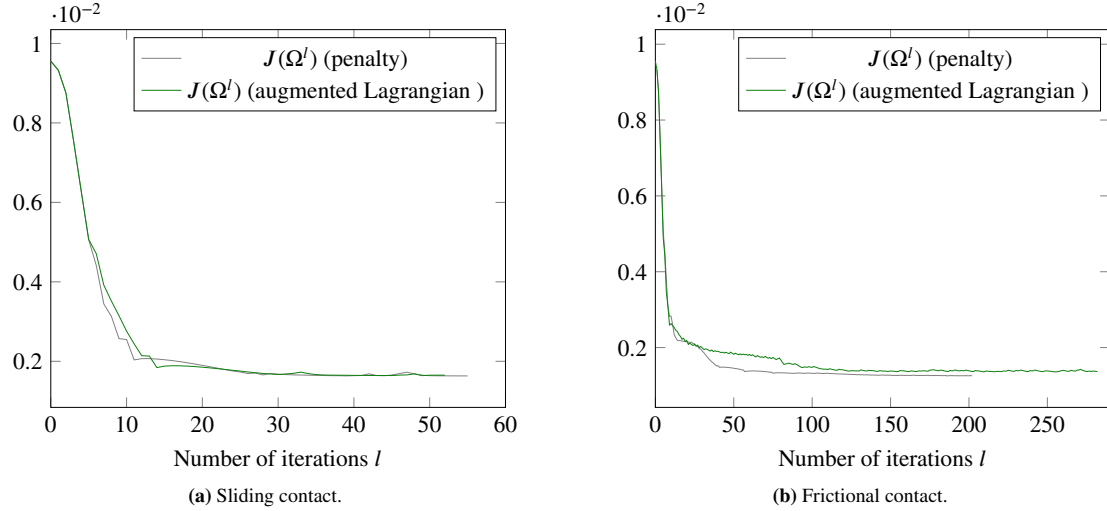


FIGURE 7 Convergence curves for the 2D bridge.

Two-dimensional cantilever in contact with a disk.

Inspired by classical shape optimization benchmarks in linear elasticity (without contact) and by benchmarks from contact problems resolution, we propose to study the case of a 2D cantilever in contact with a disk⁵⁴. This case has already been considered in shape optimization³⁸, as well as other closely related variants where the rigid body is flat^{83,84}. We prefer to consider the more general case of a disk because in the case of a plane, the normal \mathbf{n} does not depend on θ and therefore it has no influence on the shape derivative. In the works cited above, only the contact zone is optimized and this zone is represented as the graph of a finite element function on a given mesh (paradigm *discretize-then-optimize*). Here, following the paradigm *optimize-then-discretize*, we account for optimization of the whole boundary of Ω (including Γ_C) and allow changes of topology thanks to the level-set representation.

We consider the usual cantilever benchmark on the rectangle $D = [0, 2] \times [0, 1]$, where the Neumann zone Γ_N and the potential Dirichlet zone $\hat{\Gamma}_D$ are defined as in Figure 8. The only difference with the well-known case is that we add a rigid disk of radius R and center $(1, -R)$ below D . When constraints \mathbf{f} and $\boldsymbol{\tau}$ are applied, the structure might come in contact with the disk. In this

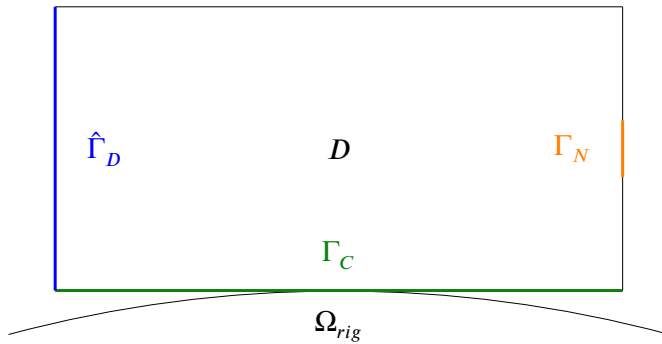


FIGURE 8 Initial geometry for the 2D cantilever in contact with a disk.

numerical example, we take $\mathbf{f} = 0$ et $\boldsymbol{\tau} = (0, -0.01)$. The coefficients of the cost functional are set to $\alpha_1 = 15$ and $\alpha_2 = 0.01$. We take $\varepsilon = 10^5$ for the penalty formulation and $\gamma_1^k = \gamma_2^k = 100$, for all k , for the augmented Lagrangian formulation. The radius

of the disk R is set to 8. Finally, in the frictional case, we take as in the previous benchmark $s = 10^{-2}$ and $\mathfrak{F} = 0.2$. With this dataset, we obtain the results displayed in Figure 9.

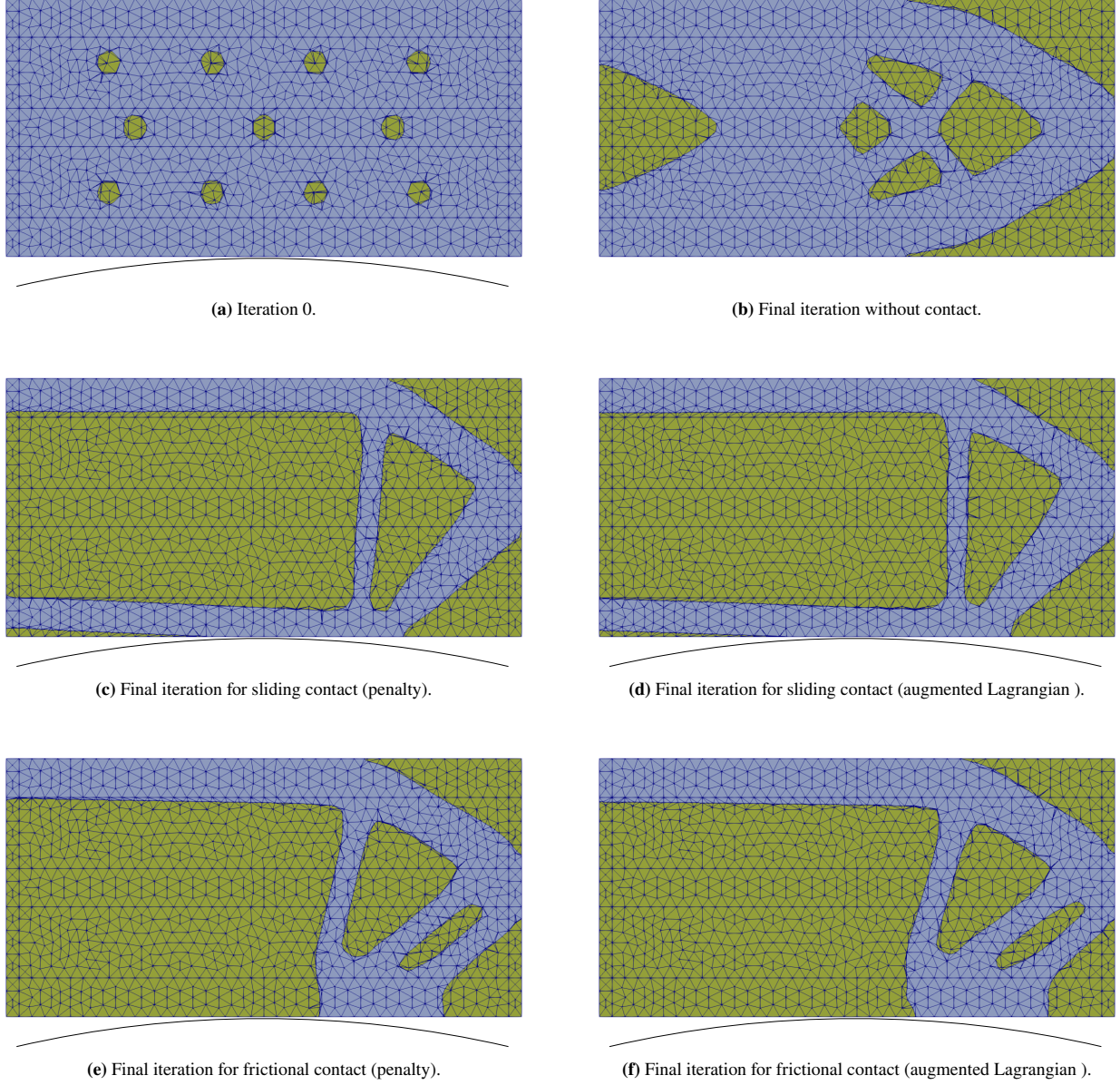


FIGURE 9 Initial and final designs for the 2D cantilever in contact with a disk (Ω_h in blue, $D_h \setminus \Omega_h$ in yellow), $\alpha_1 = 15$.

Again, we see that the penalty method and the augmented Lagrangian method give very similar final designs in the cases of sliding and frictional contact. In each case, we notice that the algorithm generated a sequence of shapes such that the location of the points in contact (initially at the center) has moved to the right during the optimization process. Indeed, when the zone where Ω is supported by Ω_{rig} gets closer to Γ_N , the structure becomes more rigid under the action of the surface load τ . For the sliding contact model, the optimal shape has two anchor zones on $\hat{\Gamma}_D$: one at the top which improves rigidity, and another at the bottom which prevents the structure to slide down to the right. For the frictional contact model, there is only one anchor zone because the structure may now stick to the rigid foundation, which improves the stability near the contact zone.

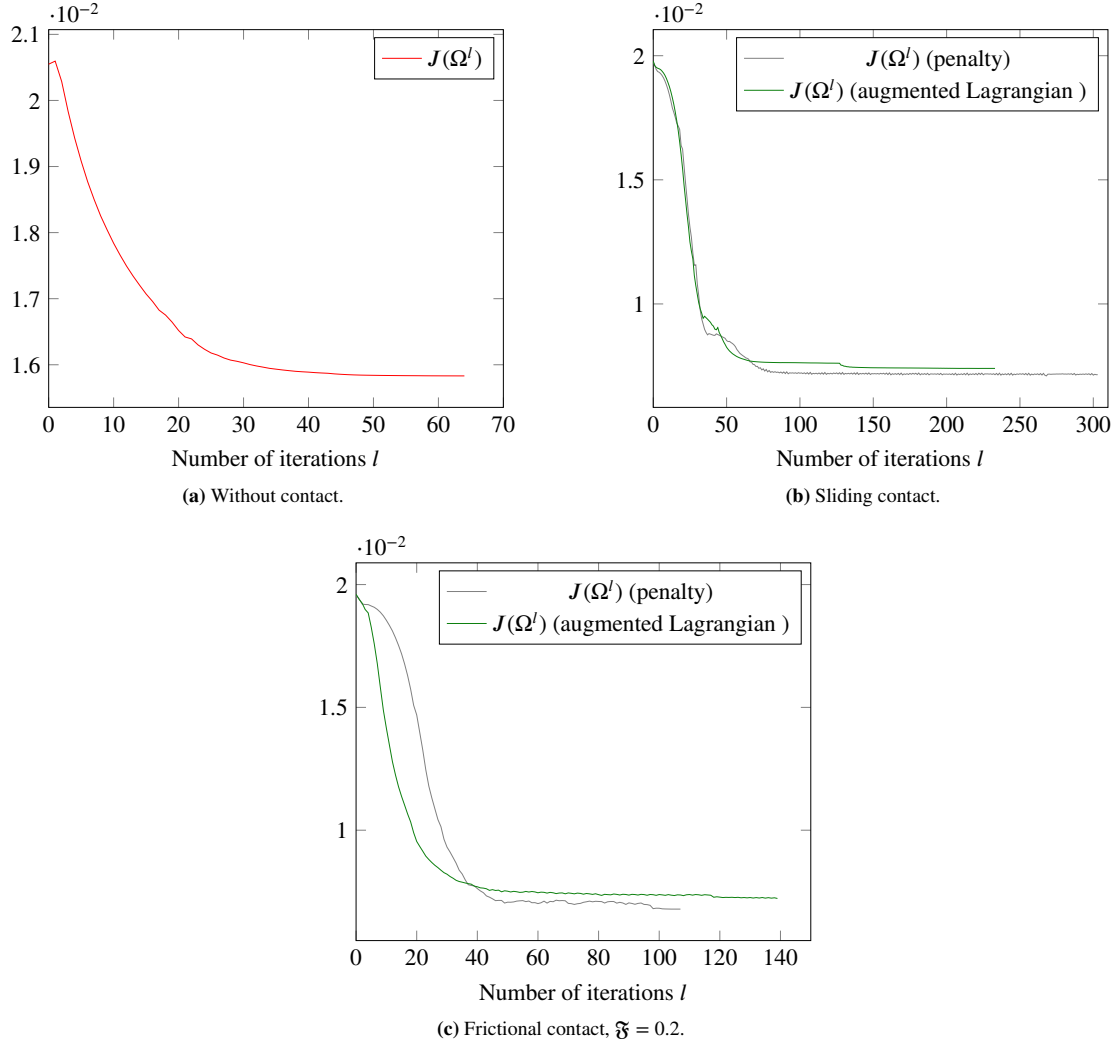


FIGURE 10 Convergence curves for the 2D cantilever in contact with a disk, $\alpha_1 = 15$.

Besides, as expected, if we compare the optimal designs obtained for the model with contact and the model without contact, we notice that thanks to the potential support offered by the rigid foundation in the case with contact, the algorithm manages to find structures which are as rigid as in the case without contact while being way lighter. This is confirmed by the values of J , see Table 2. Also note that adding friction enables us to slightly improve the value of J .

Even if the convergence histories of J (see Figure 10) reveal comparable behaviours for the penalty method and the augmented Lagrangian method, the final values are quite different. More specifically, the values in Table 2 indicate that the optimal design obtained in the penalty case is 5% more efficient than the one obtained in the augmented Lagrangian case. In fact, it seems more likely that this difference comes from the inconsistency of the penalty method since the value of the penalty parameter in this benchmark is only $\epsilon = 10^5$.

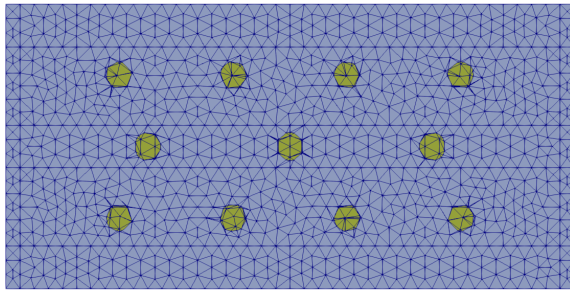
Impact of the weight coefficients.

In this paragraph, we consider the exact same benchmark as in the previous example, but we choose different weight coefficients in the shape functional. More specifically, we take here $\alpha_1 = 12$ instead of the previous choice $\alpha_1 = 15$, and we keep $\alpha_2 = 0.01$. Compared to the last example, we see that the value of α_1 is smaller, which means that we penalize less the rigidity of the structure. As shown in Figure 11, this allows the algorithm to find lighter structures, with different topologies. As for the case $\alpha_1 = 15$, we notice that the optimal structures found using the penalty formulation and the augmented Lagrangian formulation

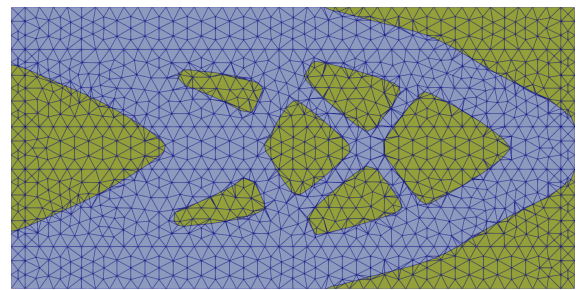
With contact	$\mathfrak{F} = 0$	$\mathfrak{F} = 0.2$	Without contact	0.0158314
Penalty	0.00714989	0.00678781		
Augmented Lagrangian	0.00740285	0.00722132		

TABLE 2 Values of J at the final iteration for the 2D cantilever, $\alpha_1 = 15$.

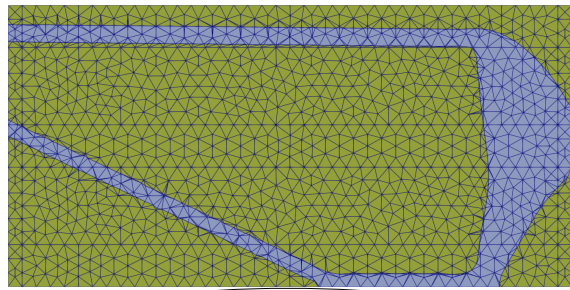
are quite similar, even though the number of anchor zones is not the same in the case of sliding contact: two for the penalty case vs one for the augmented Lagrangian case.



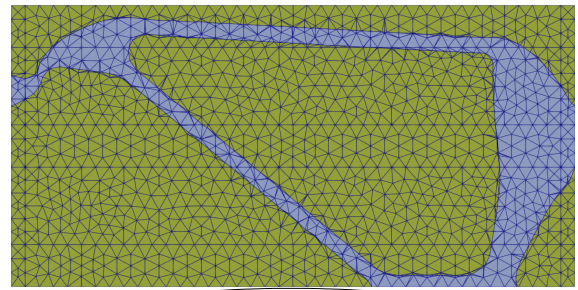
(a) Iteration 0.



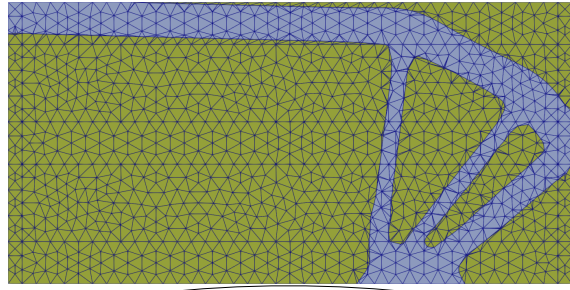
(b) Final iteration without contact.



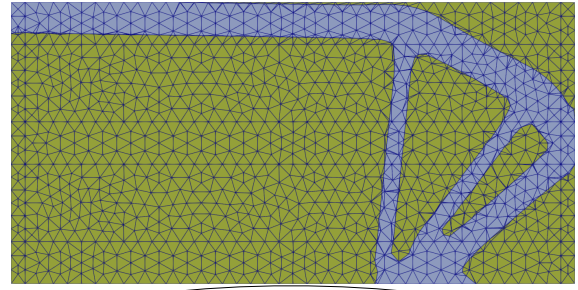
(c) Final iteration for sliding contact (penalty).



(d) Final iteration for sliding contact (augmented Lagrangian).



(e) Final iteration for frictional contact (penalty).



(f) Final iteration for frictional contact (augmented Lagrangian).

FIGURE 11 Initial and final designs for the 2D cantilever in contact with a disk, $\alpha_1 = 12$.

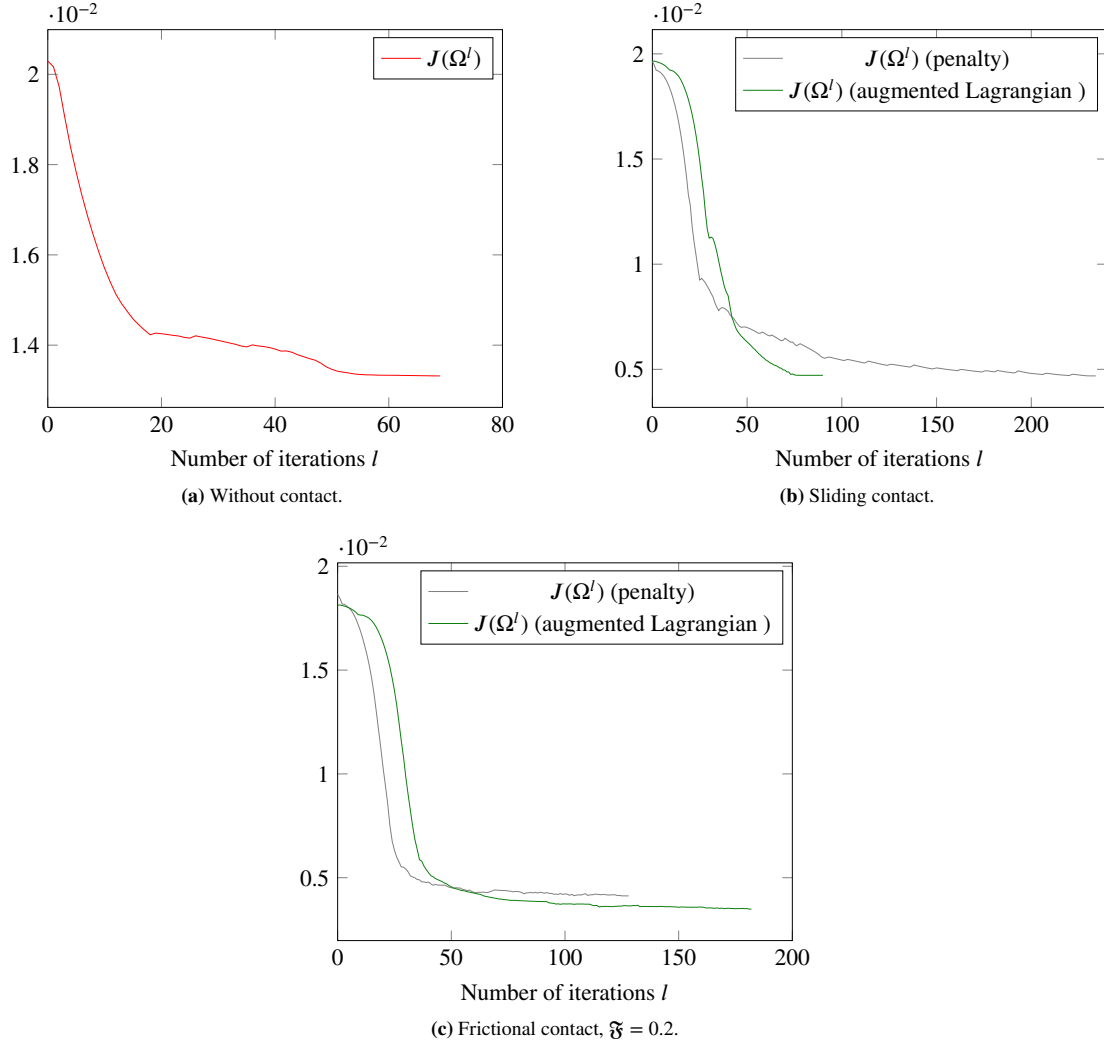


FIGURE 12 Convergence curves for the 2D cantilever in contact with a disk, $\alpha_1 = 12$.

With contact	$\mathfrak{F} = 0$	$\mathfrak{F} = 0.2$	Without contact
Penalty	0.00468765	0.00412519	0.013319
Augmented Lagrangian	0.00471535	0.00348837	

TABLE 3 Values of J at the final iteration for the 2D cantilever, $\alpha_1 = 12$.

Taking a look at the convergence curves in Figure 12 and at the values of the cost functional at the final iteration in Table 3, we see that the remarks made in the previous case still hold. Finally, these results also illustrate the robustness of the algorithm with respect to the weight coefficients α_1 and α_2 .

Three-dimensional cantilever in contact with a ball.

The three-dimensional case of optimizing the potential contact zone Γ_C for a cantilever in contact with a flat rigid foundation has also been considered⁸⁵. In this reference, the authors use the much more cumbersome Coulomb friction model and, as in the two-dimensional case, Γ_C is represented by a finite element function approximating the distance to the rigid plane. For the same reasons as in the 2D case, we suggest to consider a spherical rigid body Ω_{rig} instead of a plane. This benchmark can be

found in contact mechanics literature, though a more popular variant is the case where the ball is replaced by a cylinder which axis is orthogonal to the axis of the beam.

The domain D is a box with dimensions $5 \times 3 \times 2.4$, see Figure 15a. The potential Dirichlet $\hat{\Gamma}_D$ is the whole left side and Γ_N is a small rectangle at the center of the right side. Then, we add Ω_{rig} , a ball of radius R centered at $(2.5, -R, 1.2)$. The external forces are still given by $\mathbf{f} = 0$ and $\tau = (0, 0, -0.01)$, the Tresca threshold is set to $s = 10^{-3}$ and the friction coefficient is either $\mathfrak{T} = 0.01$ or $\mathfrak{T} = 0.05$. The parameters related to the numerical resolution are such that $\varepsilon = 10^7$ and $\gamma_1^k = \gamma_2^k = 1000$, for all k . Finally, the coefficients of J are set to $\alpha_1 = 30$, $\alpha_2 = 0.01$. In order to show the topology of the initial shape Ω at iteration 0, we have represented its complementary $D \setminus \Omega^0$ in Figure 13a.

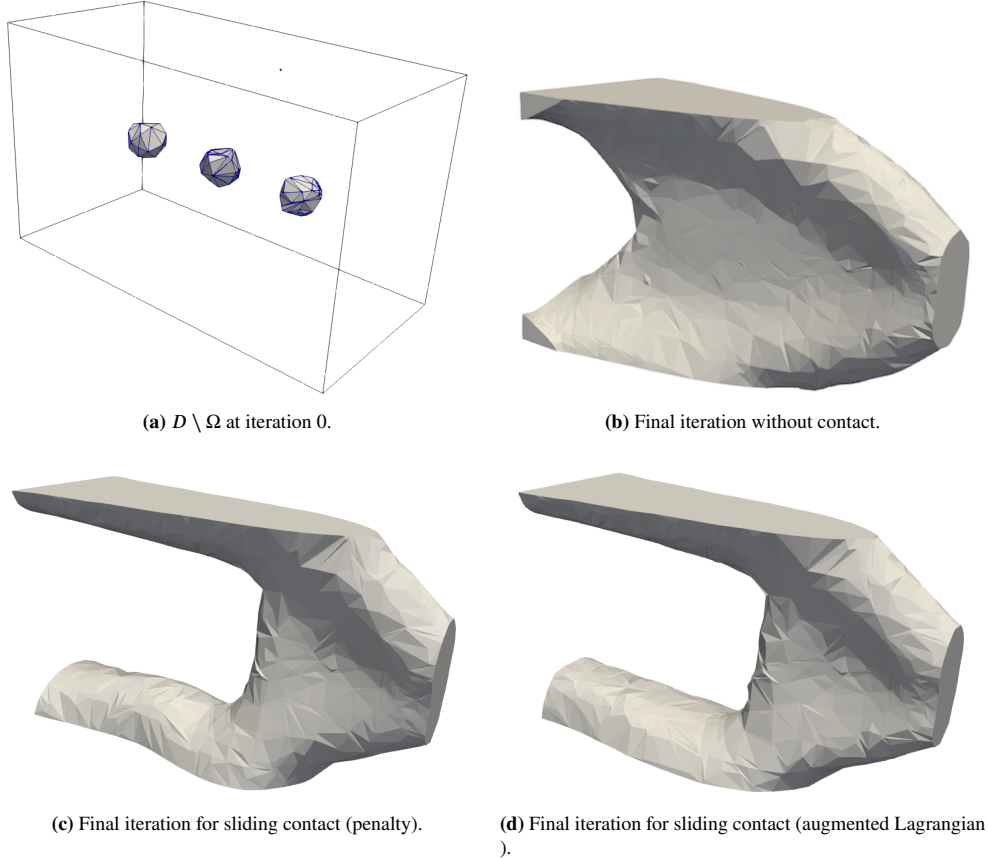


FIGURE 13 Initial and final designs for the 3D cantilever in sliding contact with a ball.

In this case as well, we obtain very similar optimal designs with the penalty and augmented Lagrangian approaches, regardless of the contact model considered (sliding or frictional), see Figure 13 and Figure 14. From the geometric point of view, the remarks made in the previous example remain valid in three dimensions: the zones where the optimal structures are supported by Ω_{rig} have been moved closer to Γ_N . As it is often the case in 3D shape optimization benchmarks, the dimension of structure in the rear-front direction has shrunk in order to make it as light as possible. Note that the coefficient α_1 in front of the compliance in the expression of J has been multiplied by two compared to the two-dimensional case and the friction coefficient is very small, which explains why all optimal designs have two anchor zones, even in the frictional case. Besides, as in the two-dimensional case, we see from Table 4 that the values of J are significantly smaller in the cases with contact compared to the case without contact, and that adding friction enables the algorithm to find slightly more efficient structures.

Remark 13. Contrary to the bidimensional case, it is possible to create "holes" in the structure in three-dimensions (such as the one in Figure 14c) by simply following the level-set propagation front. However, it is not possible to create inclusions of void in the structure (such as the three in Figure 13a), which is usually not a problem since such mechanical structures would be very

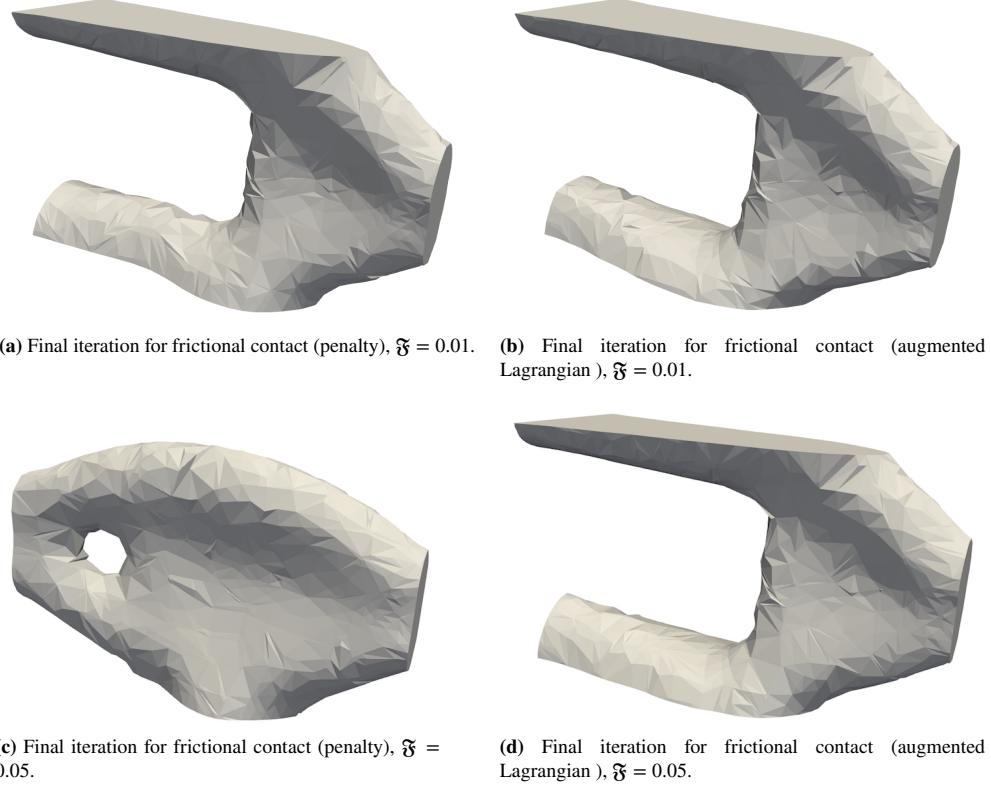


FIGURE 14 Final designs for the 3D cantilever in frictional contact with a ball.

difficult to manufacture. Nevertheless, a rather common practice in level-set based numerical shape optimization is to start with an initial design containing small inclusions^{80,25,36} in order to slightly accelerate the whole shape optimization process. When using this trick, one must be careful depending on the context as the final design might contain inclusions as well. In our case, choosing an initial design with no inclusion (Figure 15a) or with three inclusions (Figure 13a) lead to extremely similar final designs that do not contain inclusions, see Figures 15b and 13b. Besides, the convergence history in Figure 16 reveals that for the initial design containing inclusions, the algorithm converges in 97 iterations, instead of 120 iterations for the initial design with no inclusion. In addition, the two convergence curves (blue and red curves) in this figure are very close.

Finally, when looking at the convergence history of J in Figure 16, one may notice a bump around iteration 30 in the case of frictional contact with the penalty method. This corresponds to iterations where the contact zone is moved a lot and thus the Newton solver for the mechanical problem is struggling. This is also the reason why we are limited in our choice of parameters: if we take smaller values of α_1 or greater values of \mathfrak{F} , the shape might be subject to large displacements of the contact zone between two shape optimization iterations, which makes it very difficult for the Newton method to solve the penalty mechanical problem and eventually prevents the shape optimization algorithm from converging to the optimal solution. This fact has been illustrated by taking a larger friction coefficient $\mathfrak{F} = 0.05$, see Figure 14. In this case, the final structure obtained in the penalty case is very different from the one obtained in the augmented Lagrangian case, and it also leads to a greater value of J , see Table 4. In practice, we have not encountered similar difficulties with the augmented Lagrangian method, even for larger friction coefficients. In addition, the convergence of J for the augmented Lagrangian method seems smoother than the one for the penalty method in both sliding and frictional cases, which suggests that the augmented Lagrangian method is more stable from the shape optimization point of view.

Remark 14. The price to pay to work with a conforming mesh of Ω^l at each iteration l is to apply our cutting mesh procedure, which adds vertices to the mesh of the box D . In the 3D cantilever benchmark, this represents an increase of approximately 30% in the first shape optimization iterations (where Ω^l is close to $\Omega^0 \simeq D$), and up to 60% in the end of the process. On the other

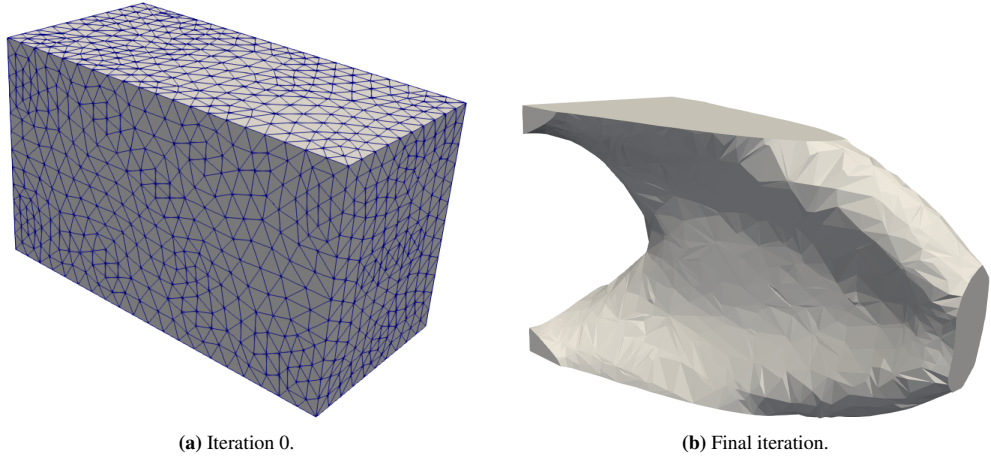


FIGURE 15 Initial design with no inclusion and final design for the 3D cantilever without contact.

With contact	$\mathfrak{F} = 0$	$\mathfrak{F} = 0.01$	$\mathfrak{F} = 0.05$	Without contact	
Penalty	0.070298	0.068989	0.0750624	Ω^0 with no inclusion	0.116407
Augmented Lagrangian	0.0724316	0.0721786	0.0708568	Ω^0 with 3 inclusions	0.116427

TABLE 4 Values of J at the final iteration for the 3D cantilever.

hand, having a conforming mesh of Ω^l at each iteration l enables us to solve only on a subdomain of D . Therefore, even though the number of vertices in D keeps increasing along the iterations, the volume of Ω^l keeps getting smaller and smaller. Thus the number of unknowns in the contact problem is decreasing along the iterations, and the computational cost to solve this problem is decreasing as well.

6 | CONCLUSION

This article presents a topology optimization algorithm based on directional shape derivatives and a level-set approach in the context of three-dimensional contact mechanics with Tresca friction. Two regularized formulations of the contact problem have been studied: the penalty formulation and the augmented Lagrangian formulation. In both cases, the expressions of the shape derivatives have been obtained at the continuous level, which makes them independent of the discretization chosen for the mechanical problem. In addition, the algorithm benefits from a simple but original mesh-cutting technique based on a quadratic interpolation of the level-set function. This enables us to have a mesh of the discrete domain at each iteration and thus apply the contact conditions exactly on Γ_C . Finally, the validity of our approach has been illustrated in three numerical examples. The results suggest that the augmented Lagrangian method is more stable and robust than the penalty method in the context of shape optimization, especially in three-dimensions.

A natural extension of this work would be to consider the more realistic Coulomb friction model. Of course, there is a huge gap in terms of theoretical and numerical difficulties between the Tresca model and the Coulomb model. However, it is known⁴¹ that under some specific assumptions, the solution to the Coulomb problem can be approximated by a fixed point method which solves a Tresca problem at each iteration. From the numerical point of view, it might be necessary in this case to include a post-processing remeshing procedure in our algorithm in order to improve the quality of the mesh after cutting it.

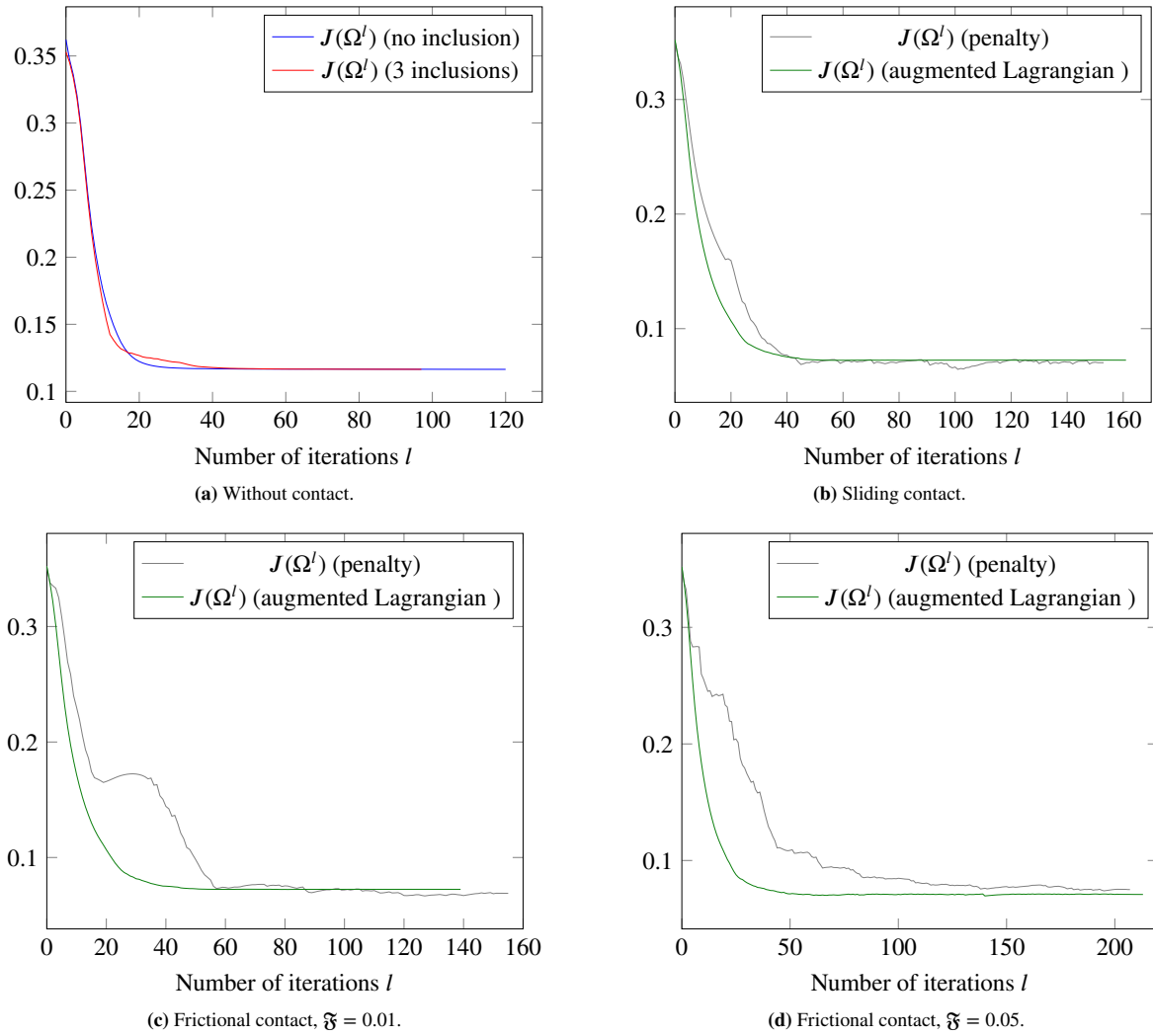


FIGURE 16 Convergence curves for the 3D cantilever in contact with a ball.

ACKNOWLEDGMENTS

This work was supported by the Natural Sciences and Engineering Research Council of Canada (NSERC).

References

- Chaudet-Dumas B, Deteix J. Shape derivatives for the penalty formulation of elastic contact problems with Tresca friction. *SIAM Journal on Control and Optimization* 2020; 58(6): 3237–3261.
- Chaudet-Dumas B, Deteix J. Shape derivatives for an augmented Lagrangian formulation of elastic contact problems. *ESAIM: Control, Optimisation and Calculus of Variations* 2021; 27: S14.
- Li S, Petzold L. Adjoint Sensitivity Analysis for Time-Dependent Partial Differential Equations with Adaptive Mesh Refinement. *Journal of Computational Physics* 2004; 198(1): 310-325. doi: 10.1016/j.jcp.2003.01.001
- Heinemann C, Sturm K. Shape optimization for a class of semilinear variational inequalities with applications to damage models. *SIAM Journal on Mathematical Analysis* 2016; 48(5): 3579–3617.

5. Allaire G, Jouve F, Toader AM. Structural optimization using sensitivity analysis and a level-set method. *Journal of computational physics* 2004; 194(1): 363–393.
6. Bendsoe M, Sigmund O. *Topology Optimization: Theory, Methods, and Applications*. Engineering Online Library Springer Berlin Heidelberg . 2003.
7. Hadamard J. *Mémoire sur le problème d'analyse relatif à l'équilibre des plaques élastiques encastrées*. 33. Imprimerie nationale . 1908.
8. Murat F, Simon J. Étude de problèmes d'optimal design. In: Springer. ; 1975: 54–62.
9. Simon J. Differentiation with respect to the domain in boundary value problems. *Numerical Functional Analysis and Optimization* 1980; 2(7-8): 649–687.
10. Pironneau O. Optimal shape design for elliptic systems. In: Springer. 1982 (pp. 42–66).
11. Sokolowski J, Zolésio JP. Introduction to shape optimization. In: Springer. 1992.
12. Delfour MC, Zolésio JP. *Shapes and Geometries: Analysis, Diefferential Calculus, and Optimisation*. Philadelphia, PA: Society for Industrial and Applied Mathematics . 2001.
13. Henrot A, Pierre M. *Variation et optimisation de formes: une analyse géométrique*. 48. Springer Science & Business Media . 2006.
14. Sethian JA, Wiegmann A. Structural boundary design via level set and immersed interface methods. *Journal of computational physics* 2000; 163(2): 489–528.
15. Osher SJ, Santosa F. Level set methods for optimization problems involving geometry and constraints: I. Frequencies of a two-density inhomogeneous drum. *Journal of Computational Physics* 2001; 171(1): 272–288.
16. Wang MY, Wang X, Guo D. A level set method for structural topology optimization. *Computer methods in applied mechanics and engineering* 2003; 192(1-2): 227–246.
17. Yulin M, Xiaoming W. A level set method for structural topology optimization and its applications. *Advances in Engineering software* 2004; 35(7): 415–441.
18. Allaire G, De Gournay F, Jouve F, Toader AM. Structural optimization using topological and shape sensitivity via a level set method. *Control and cybernetics* 2005; 34(1): 59.
19. Van Dijk NP, Maute K, Langelaar M, Van Keulen F. Level-set methods for structural topology optimization: a review. *Structural and Multidisciplinary Optimization* 2013; 48(3): 437–472.
20. Belytschko T, Xiao SP, Parimi C. Topology optimization with implicit functions and regularization. *International Journal for Numerical Methods in Engineering* 2003; 57(8): 1177–1196.
21. Kreissl S, Maute K. Levelset based fluid topology optimization using the extended finite element method. *Structural and Multidisciplinary Optimization* 2012; 46(3): 311–326.
22. Ha SH, Cho S. Level set based topological shape optimization of geometrically nonlinear structures using unstructured mesh. *Computers & Structures* 2008; 86(13-14): 1447–1455.
23. Yamasaki S, Nomura T, Kawamoto A, Sato K, Nishiwaki S. A level set-based topology optimization method targeting metallic waveguide design problems. *International Journal for Numerical Methods in Engineering* 2011; 87(9): 844–868.
24. Allaire G, Dapogny C, Frey P. Topology and geometry optimization of elastic structures by exact deformation of simplicial mesh. *Comptes Rendus Mathematique* 2011; 349(17-18): 999–1003.
25. Allaire G, Dapogny C, Frey P. Shape optimization with a level set based mesh evolution method. *Computer Methods in Applied Mechanics and Engineering* 2014; 282: 22–53.

26. Abe K, Kazama S, Koro K. A boundary element approach for topology optimization problem using the level set method. *Communications in numerical methods in Engineering* 2007; 23(5): 405–416.
27. Duvaut G, Lions JL. *Les inéquations en mécanique et en physique*. Paris: Dunod . 1972.
28. Boieri P, Gastaldi F, Kinderlehrer D. Existence, uniqueness, and regularity results for the two-body contact problem. *Applied Mathematics and Optimization* 1987; 15(1): 251–277.
29. Mignot F, Puel JP. Optimal control in some variational inequalities. *SIAM Journal on Control and Optimization* 1984; 22(3): 466–476.
30. Sokółowski J, Zolésio JP. Shape sensitivity analysis of contact problem with prescribed friction. *Nonlinear Analysis: Theory, Methods & Applications* 1988; 12(12): 1399–1411.
31. Kočvara M, Outrata J. On optimization of systems governed by implicit complementarity problems. *Numerical Functional Analysis and Optimization* 1994; 15(7-8): 869–887.
32. Beremlijski P, Haslinger J, Kočvara M, Outrata J. Shape optimization in contact problems with Coulomb friction. *SIAM Journal on Optimization* 2002; 13(2): 561–587.
33. Haslinger J, Outrata J, Pathó R. Shape optimization in 2D contact problems with given friction and a solution-dependent coefficient of friction. *Set-Valued and Variational Analysis* 2012; 20(1): 31–59.
34. Beremlijski P, Haslinger J, Outrata J, Pathó R. Shape optimization in contact problems with Coulomb friction and a solution-dependent friction coefficient. *SIAM Journal on Control and Optimization* 2014; 52(5): 3371–3400.
35. Kim NH, Choi KK, Chen JS, Park YH. Meshless shape design sensitivity analysis and optimization for contact problem with friction. *Computational Mechanics* 2000; 25(2-3): 157–168.
36. Maury A, Allaire G, Jouve F. Shape optimisation with the level set method for contact problems in linearised elasticity. *SMAI-Journal of computational mathematics* 2017; 3: 249–292.
37. Fancello E, Feijóo R. Shape optimization in frictionless contact problems. *International journal for numerical methods in engineering* 1994; 37(13): 2311–2335.
38. Fancello EA, Haslinger J, Feijoo RA. Numerical comparison between two cost functions in contact shape optimization. *Structural Optimization* 1995; 9(1): 57–68.
39. Bretin E, Chapelat J, Outtier PY, Renard Y. Shape optimization of a linearly elastic rolling structure under unilateral contact using Nitsche's method and cut finite elements. *Computational Mechanics* 2022: 1–20.
40. Chouly F, Hild P. A Nitsche-based method for unilateral contact problems: numerical analysis. *SIAM Journal on Numerical Analysis* 2013; 51(2): 1295–1307.
41. Eck C, Jarusek J, Krbec M. *Unilateral contact problems: variational methods and existence theorems*. CRC Press . 2005.
42. Kikuchi N, Oden JT. *Contact problems in elasticity: a study of variational inequalities and finite element methods*. 8. SIAM . 1988.
43. Jarušek J. Contact problems with bounded friction. Coercive case. *Czechoslovak Mathematical Journal* 1983; 33(2): 237–261.
44. Eck C, Jarusek J. Existence results for the static contact problem with Coulomb friction. *Mathematical Models and Methods in Applied Sciences* 1998; 8(03): 445–468.
45. Hild P. Non-unique slipping in the coulomb friction model in two-dimensional linear elasticity. *Quarterly Journal of Mechanics and Applied Mathematics* 2004; 57(2): 225–235.

46. Hild P. Multiple solutions of stick and separation type in the Signorini model with Coulomb friction. *ZAMM-Journal of Applied Mathematics and Mechanics/Zeitschrift für Angewandte Mathematik und Mechanik: Applied Mathematics and Mechanics* 2005; 85(9): 673–680.
47. Renard Y. A uniqueness criterion for the Signorini problem with Coulomb friction. *SIAM journal on mathematical analysis* 2006; 38(2): 452–467.
48. Lions JL, Stampacchia G. Variational inequalities. *Communications on pure and applied mathematics* 1967; 20(3): 493–519.
49. Laborde P, Renard Y. Fixed point strategies for elastostatic frictional contact problems. *Mathematical methods in the applied sciences* 2008; 31(4): 415–441.
50. Oden JT, Kikuchi N. Theory of variational inequalities with applications to problems of flow through porous media. *International Journal of Engineering Science* 1980; 18(10): 1173–1284.
51. Ciarlet PG. *Mathematical Elasticity Vol. 1 : Three-Dimensional Elasticity*. North-Holland Pub. Co. . 1988.
52. Ekeland I, Temam R. *Convex analysis and variational problems*. 28. Siam . 1999.
53. Ito K, Kunisch K. *Lagrange multiplier approach to variational problems and applications*. SIAM . 2008.
54. Stadler G. *Infinite-dimensional semi-smooth Newton and augmented Lagrangian methods for friction and contact problems in elasticity*. Selbstverl. . 2004.
55. Courant R. Variational methods for the solution of problems of equilibrium and vibrations. *Bulletin of the American Mathematical Society* 1943; 49(1): 1–23.
56. Kikuchi N, Song YJ. Penalty/Finite-Element Approximations of a Class of Unilateral Problems in Linear Elasticity. *Quarterly of Applied Mathematics* 1981; 39(1): 1–22.
57. Wriggers P, Simo JC, Taylor RL. Penalty and Augmented Lagrangian Formulations for Contact Problems. *Numerical Methods in Engineering: Theory and Applications* 1985.
58. Simons JW, Bergan PG. A Finite Element Formulation of Three-Dimensional Contact Problems with Slip and Friction. *Computational Mechanics* 1986.
59. Chaudet-Dumas B. *Optimisation de formes pour les problèmes de contact en élasticité linéaire*. PhD thesis. Université Laval, Québec, Canada; 2019.
60. Chouly F, Hild P. On convergence of the penalty method for unilateral contact problems. *Applied Numerical Mathematics* 2013; 65: 27–40.
61. Hestenes MR. Multiplier and Gradient Methods. *Journal of Optimization Theory and Applications* 1969; 4(5): 303–320.
62. Powell MJD. A Method for Nonlinear Constraints in Minimization Problems. In: Fletcher R., ed. *Optimization* New York: Academic Press. 1969 (pp. 283–298).
63. Landers J, Taylor R. An Augmented Lagrangian Formulation for the Finite Element Solution of Contact Problems. tech. rep., California Univ Berkeley Dept of Civil Engineering; California, USA: 1986.
64. Alart P, Curnier A. A Mixed Formulation for Frictional Contact Problems Prone to Newton like Solution Methods. *Computer Methods in Applied Mechanics and Engineering* 1991; 92(3): 353 - 375. doi: [https://doi.org/10.1016/0045-7825\(91\)90022-X](https://doi.org/10.1016/0045-7825(91)90022-X)
65. Simo JC, Laursen TA. An Augmented Lagrangian Treatment of Contact Problems Involving Friction. *Computers and Structures* 1992; 42(1): 97 - 116. doi: [https://doi.org/10.1016/0045-7949\(92\)90540-G](https://doi.org/10.1016/0045-7949(92)90540-G)
66. Laursen T, Simo J. Algorithmic Symmetrization of Coulomb Frictional Problems Using Augmented Lagrangians. *Computer Methods in Applied Mechanics and Engineering* 1993; 108: 133-146.

67. Heegaard JH, Curnier A. An Augmented Lagrangian Method for Discrete Large-Slip Contact Problems. *International Journal for Numerical Methods in Engineering* 1993; 36(4): 569–593. doi: 10.1002/nme.1620360403
68. Ito K, Kunisch K. Augmented Lagrangian methods for nonsmooth, convex optimization in Hilbert spaces. *Nonlinear Analysis: Theory, Methods & Applications* 2000; 41(5-6): 591–616.
69. Céa J. Conception optimale ou identification de formes, calcul rapide de la dérivée directionnelle de la fonction coût. *ESAIM: Mathematical Modelling and Numerical Analysis* 1986; 20(3): 371–402.
70. Stadler G. Semismooth Newton and augmented Lagrangian methods for a simplified friction problem. *SIAM Journal on Optimization* 2004; 15(1): 39–62.
71. Osher S, Sethian JA. Front Propagating with Curvature Dependent Speed: Algorithms Based on Hamilton-Jacobi Formulations. *Journal of Computational Physics* 1988; 79: 12–49.
72. Allaire G, Jouve F, Toader AM. A level-set method for shape optimization. *Comptes Rendus Mathematique* 2002; 334(12): 1125–1130.
73. Burman E, Hansbo P, Larson MG. Augmented Lagrangian finite element methods for contact problems. *ESAIM: Mathematical Modelling and Numerical Analysis* 2019; 53(1): 173–195.
74. Chouly F. An adaptation of Nitsche method to the Tresca friction problem. *Journal of Mathematical Analysis and Applications* 2014; 411(1): 329–339.
75. De Gournay F. Velocity extension for the level-set method and multiple eigenvalues in shape optimization. *SIAM journal on control and optimization* 2006; 45(1): 343–367.
76. Dapogny C. *Shape optimization, level set methods on unstructured meshes and mesh evolution*. PhD thesis. Université Pierre et Marie Curie-Paris 6, Paris; 2013.
77. Harten A, Osher S. Uniformly high-order accurate nonoscillatory schemes. I. *SIAM Journal on Numerical Analysis* 1987; 24(2): 279–309.
78. Osher S, Shu CW. High-order essentially nonoscillatory schemes for Hamilton–Jacobi equations. *SIAM Journal on numerical analysis* 1991; 28(4): 907–922.
79. Lorensen WE, Cline HE. Marching cubes: A high resolution 3D surface construction algorithm. In: . 21. ACM. ; 1987: 163–169.
80. Allaire G, Dapogny C, Frey P. A mesh evolution algorithm based on the level set method for geometry and topology optimization. *Structural and Multidisciplinary Optimization* 2013; 48(4): 711–715.
81. Strömbärg N, Klarbring A. Topology optimization of structures in unilateral contact. *Structural and Multidisciplinary Optimization* 2010; 41(1): 57–64.
82. Maury A. *Shape optimization for contact and plasticity problems thanks to the level set method*. PhD thesis. Université Pierre et Marie Curie-Paris VI, Paris; 2016.
83. Haslinger J, Neittaanmäki P. Shape optimization in contact problems. Approximation and numerical realization. *ESAIM: Mathematical Modelling and Numerical Analysis* 1987; 21(2): 269–291.
84. Haslinger J, Mäkinen RAE. *Introduction to shape optimization: theory, approximation, and computation*. SIAM . 2003.
85. Beremlijski P, Haslinger J, Kočvara M, Kučera R, Outrata JV. Shape optimization in three-dimensional contact problems with Coulomb friction. *SIAM Journal on Optimization* 2009; 20(1): 416–444.

